JAERI-M
82-145

PROGRESS REPORT ON SAFETY RESEARCH OF HIGH-LEVEL WASTE MANAGEMENT FOR THE PERIOD APRIL, 1981 TO MAY, 1982

October 1982

(Ed.) Shingo TASHIRO

日本原子力研究所
Japan Atomic Energy Research Institute

8303180126 830302
PDR WASTE
WM-1 PDR

JAERI-M 82-145

Progress Report on Safety Research of High-Level Waste Management for The Period April, 1981 to May, 1982

(Ed.) Shingo TASHIRO

Division of Environmental Safety Research,
Tokai Research Establishment, JAERI

(Received September 28, 1982)

Main results obtained on Safety Research of High-Level Waste Management in 1981 were edited.

The research theme are following.

(1) Characterization of vitrified waste
(2) Alternative waste form development
(3) Durability tests for HLW storage facility
(4) Safety evaluation of geologic disposal
(5) Preparation for hot test

Keywords: High-level Waste, Glass Form, Characterization, Storage Facility, Geological Disposal, Safety Estimation, Hot Test, Progress Report

Contents

Introduction

S. Tashiro

Safety assessment studies are strongly required to verify whether the developed scenarios for high-level waste management can be safely adapted to Japanese circumstances at the present stage of designing a pilot plant for the vitrification and storage and of discussing the specification of to-be-returned wastes from the oversea reprocessing.

The Japan Atomic Energy Commission has revised the development schedule for high-level waste management in 1980 and is expecting the Japan Atomic Energy Research Institute (JAERI) to play a role in the safety studies as a verifier.

JAERI started studies on high-level waste management nearly ten years ago, and has focussed the studies on two subjects that are to develop the methods for the safety assessment during the storage and disposal and to compile data for the assessment. It is essential for the data compilation to clarify the pass ways of the waste release to the environment and to examine the performance of each barrier against the release.

This report reviews main results obtained in the last fiscal year (F.Y.) of 1981 (from April, 1981 to March, 1982) as a progress report on safety research of High-Level Waste Management in JAERI. Besides the main studies, it was also important to extend to examinations with real radioactivity using the Waste Safety Testing Facility (WASTEF) to start hot run in Autumn of 1982.

Remarks

S. Muraoka and M. Senoo

Characterization of high level radioactive waste (HLW) product has been studied using simulated HLW as the main subject of the High Level Waste Management Laboratory since 1973. Many characteristics are necessitated for safety estimation of each step of HLW management, i.e. tansportation, storage or disposal.

For almost all of the characteristics, the suitable methods have been developed on cold stage being aimed to adapt to hot test, for example, leach rate both in normal and in high-temperature condition, thermal conductivity, devitrifying property, homogenity, and mechanical resistance in the events of dropping and rapid cooling.

Leaching and devitrifying mechanism of the HLW glass have been studied on the stand point of long term storage.

Development of alternative HLW form is now concentrated on rock form solidification, just like as SYNROC products. The solidifing conditions are being developed based on the results from the characteristics examination. After the preliminary study, engineering scale test will be started in 1986.

Durability tests of materials to be used for construction of storage facility were started newly in the year for to-be-returned wastes arisen from oversea reprocessing. The test in the year did not show remarkable change of mechanical strength of concrete materials due to γ-ray irradiation but showed a effect of temperature of the atmosphere. For canister materials, it is clarified that the susceptibility to SCC was promoted by γ-ray irradiation in some alloys. The tests will be continued in the next year.

Safety evaluation of geologic disposal, one of the essential subjects in the laboratory, was started in 1977. This study is constituted by two kinds of approach that are estimation by computer codes and examination by experiments.

Regarding to the estimation study by computor code, calculation about nuclide migration in geoshere and stress

around the repository has been started.

Experiments on nuclide behavior in rock formation have been carried out in laboratory and field. The comparison between the both data should show a interesting result. Such approach will give a clue to establish a total system of the safety assessment in future.

Preparation for examination using radioactive materials has been carried out in parallel with construction of the Waste Safety Testing Facility (WASTEF).

Main items of the examination are series of tests of vitrified forms under the proposed condition of storage and disposal.

The test will be advanced from a cold test at first, secondarily to semi-hot test using radioactivity, and finally to demonstrative hot test using real HLW.

Through the tests, many useful data will be obtained, which would make clear the acceptable limits of the characteristics of vitrified HLW for a safe management system.

1. Glass form examination

1.1 Leaching Mechanism

T. Banba

The glass matrix is the primary barrier to immobilize radioactive nuclides in the high level waste (HWL) repository configuration. Leaching mechanism of the waste glass have been studied by many workers.[1,2)]

Surface layer on the leached glass is liable to act as an important factor on leaching mechanism, which were studied by D. M. Strachan[3)] and other workers.[4,5)] In present work constituents of the layer was examined and its function was discussed on leaching surface of glass blocks in order to clarify leaching mechanism in glass cracks.

(1) Formation of surface layers

Experimental

The investigated waste glass was a borosilicate glass (J-10) with 14 wt% waste oxides, composition of which is shown in Table 1-1. Shape of the sample was a hexahedron of 7.3 × 6.5 × 4.5 mm, and the weight was about 0.6 grams. The leach test was carried out by using a quartz Soxhlet extraction leach test apparatus for 200 days. The leachate solutions were quantitatively analyzed by means of the inductively coupled argon plasma instrument (ICP) and the atomic absorption analysis. The leached sample was washed, and dried. The sample fixed in resin was polished by Alumina and diamond paste. The leached surfaces were analyzed by optical microscopy, scanning electron microscopy (SEM), and electron probe micro analysis (EPMA).

Results and Discussion

The time dependence of leached fraction of each element is shown in Fig. 1-1. And analysis of the leachate solution for 21 elements showed that 14 elements (B, Na, Mg, Al, Ca, Ti, Cr, Fe, Sr, Y, Zr, Mo, Cs, Ba) could be detected. However, Mg, Ti, Fe, Y, and Zr were found in solution at

concentrations 10^2 to 10^5 times lower than the other elements.

The bulk glass which remained after leached for 200 days had the size of 5.70 × 4.85 × 2.95 mm and the weight of 0.2125 g. Therefore, the specific weight loss is about 63%. Fractional releases of Cs, B, Mo, and Na are almost the same as the specific weight loss after leached for 200 days. Releases of Ba, Sr, and Ca are less than those of above elements and fractional releases are about 50 wt%. The values of Cr and Al are also small (~40wt%).

The sample leached for 200 days at 100°C is covered by a gel layer. A micrograph of this surface layer is shown in Fig. 1-2. Careful examination of the photomicrograph shows this surface layer is composed of at least five distinct phases. The thickness of this layer is about 550 μm.

The relative concentrations in this layer are shown in Fig. 1-3 in the form of X-ray line scans, each element profile obtained at the white line in a SEM-micrograph of the surface layer. In the leached surface layer of the sample, Si increases with depth to the composition of the bulk glass. Also Ca was found more at the inner portion in the surface layer. Al was found to be slightly depleted in the surface layer relative to the bulk glass but its concentration in the surface layer changes little. Na was found to be depleted from the surface layer, as were Cs and Mo. Contents of Fe and Ce are higher in the surface layer, particularly the outer portion, relative to the bulk glass. The rare earth elements, Ni, Cr, Zr, and Mn have the profiles similar to these of Fe and Ce.

Although the leaching mechanism strictly differ with leached elements, it is clarified from this experiment that the leaching mechanism can be considered by classifying the leached elements into at least three groups; the elements of first group (Na etc.) are depleted through the surface layer, the elements of second group (Si, Ca etc.) are remained in the inner portion of surface layer, and the elements of third group (Fe, Ce etc.) are enriched in

the outer portion of surface layer because other groups leave from the layer. On the basis of these facts, the research is in progress to establish leaching mechanisms and to develop mathematical models of leaching.

(2) Leaching behavior in the contacting surface of waste glass

In the leaching experiment on three glass samples set in piles, it was found that the leach of the samples proceeded with a wedge along by the contacting surface. In this paper, this experimental results are described and the simple calculation model for estimation of leaching figure in the contacting surface is studied.

Experimental

Table 1-2 shows a composition of a simulated high-level waste glass used for this leaching experiment. This waste glass has the composition as produced by AVM process in France. The shape of samples is cube of 5 × 5 × 5 mm. The leaching was carried out by a Pylex Soxhlet extraction leaching apparatus. In this experiment, three samples were set in piles. The leaching was carried out for 18 days. The samples were washed and dried after leaching and then the surfaces of the samples were observed by a magnifier and an optical microscope.

Experimental Results

Fig. 1-4 shows the contacting surfaces of three piled samples after leaching test for 18 days at 100°C. It was found that the center portions of the contacting surfaces are dissolute little and that the outer portions are covered by a gel layer. The sectional shape of the leached sample is shown in Fig. 1-5, where a broken line shows the shape of nonleached sample.

Leaching model for calculation

The mathematical model of leaching is illustrated in Fig. 1-6. The leaching model is devised in order to analize the change of contacting surface of the piled samples. This model is proposed based on the following assumptions on the stand point that threshold rate of dissolution is due to diffusion of the second group described in section 1.1, especially SiO_2.

1) SiO_2 concentration of the external water is constant and 0.
2) SiO_2 concentration in gap between the piled samples changes by diffusion and dissolution.
3) The initial SiO_2 concentration in gap is assumed to be equal to the SiO_2 concentration in saturated solution; C_o.
4) Dissolution of glass proceeds in the derection of y in proportion to the difference between the equilibrium concentration of glass-water and SiO_2 concentration in gap.
5) At the external surfaces of glss, glass dissolutes at a constant rate; R.
6) Diffusion coefficient in the gel surface layer is assumed to be equal to that in gap water.

Calculation

Consider the diffusion of SiO_2 in the gap of contacting surface. Now, taking the mass balance of small volume v shown in Fig. 1-7 the following equation is obtained;

$$(y + \frac{dy}{2}) \cdot 1 \cdot dx \frac{\partial c}{\partial t} = y \cdot 1 \cdot F_x - (y + dy) \cdot 1 \cdot (F_x + \frac{\partial F_x}{\partial x} dx) \quad (1)$$

If equation (1) is rearranged by using Fick's law; $F_x = -D \frac{\partial c}{\partial x}$, it becomes the following equation.

$$\frac{\partial c}{\partial t} \approx D \frac{\partial^2 c}{\partial x^2} \left(1 + \frac{dy}{2y}\right) + \frac{\partial c}{\partial x} \frac{dy}{dx} \frac{D}{y} \left(1 - \frac{dy}{2y}\right) \tag{2}$$

Where x and y represent the coordinates, F_x is the mass transfer rate per unit area, c is the concentration, t is the time, and D is the diffusion coefficient.

Then consider the dissolution in the derection of y. If a equilibrium constant on the contacting surface of glass and water E is defined by the following equation (3), the dissolution rate becomes equation (4).

$$c_{eq} = Ec_g \tag{3}$$

$$\frac{\partial y}{\partial t} = K(Ec_g - c) \frac{1}{c_g} \tag{4}$$

Where c_{eq} is SiO_2 concentration is saturated solution, c_g is SiO_2 concentration is glass, and K is the film mass transfer coefficient. The concentration increase in the gap is given in a form of the following equation.

$$\frac{\partial c}{\partial t} = \frac{1}{(y + dy)} \cdot \frac{\partial y}{\partial t} \cdot c_g \tag{5}$$

Numerical solutions for the system of equations (2), (4) and (5) are obtained as follows:

$$C_{i,j+1} = C_{i,j} + DX\{(C_{i+1,j} - 2C_{i,j} + C_{i-1,j})(1+DY) + 2(C_{i+1,j} - C_{i,j})DY(1-DY)\} \tag{6}$$

where $DY = \frac{Y_{i,j} - Y_{i,j-1}}{2Y_{i,j}}$ and $DX = \frac{\Delta T}{(\Delta X)^2}$

$$Y_{i,j+1} = Y_{i,j} + \Delta T \cdot K' \cdot E(1 - C_{i,j+1}) \tag{7}$$

$$C_{i,j+1} = C_{i,j} + \frac{1}{Y_{i,j+1}} \cdot \Delta T \cdot K'(1 - C_{i,j+1}) \tag{8}$$

The computer program was designed by using equations (6), (7) and (8). Fig. 1-8 shows the flow sheet of the program.

Calculated results

Results computed by use of this program are shown in Fig. 1-9. In the calculations, the values (dissolution rate; R, SiO_2 concentration in glass; c_g, SiO_2 concentration in saturated solution; C_o, film mass transfer coefficient; K, and size of sample; ℓ) obtained by experiments were used for input data except for diffusion coefficient; D and initial gap width; Y_o. It was found that the result computed under the condition of $D = 1.8 \times 10^{-5}$ m²/h and $Y_o = 1.0 \times 10^{-5}$m agrees well with the experimental values.

Reference

1) R.H. Doremus, "Time Dependence of the Reaction of Water with Glass" Nuclear and Chemical Waste Management, 2, 119 (1981)
2) A.J. Machiels and C. Pescatore, "The Influence of Surface Processes in Waste Form Leaching," Scientific Basis for Nucl. Waste Management, 3, 371 (1981)
3) D.M. Strachen, et al., "MCC-1: A Standard Leach Test for Nuclear Waste Forms," Nucl. Techno. 56, 306 (1982)
4) F.K. Altenhein, et al., "The Mechanisms for Hydrothermal Leaching of Glass and Glass-Ceramic Nuclear Waste Forms," Scientific Basis for Nucl. Waste Management, 3, 363 (1981)
5) G.G. Wicks, et al., "Durability of Simulated Waste Glass-Effects of Pressure and Formation of Surface Layers" DP-MS-81-25(1981)

1.2 Devitrification of a simulated high-level waste glass containing the elements of platinum group

H. Mitamura

High-level wastes (HLW's) contain the elements of platinum group which are liable to be segregated in HLW glasses[1]. Devitrification of the glasses is prompted by action of these segregated materials as nuclei[2]. Function of the elements of platinum group for the devitrification of a borosilicate glass containing a simulated HLW was studied.

Experiment

The compositions of a simulated HLW and a borosilicate glass frit are given in Table 1-3 and 1-4 respectively. A simulated HLW glass (W-glass) included 20 wt% waste oxides. A reference glass (R-glass) excluded only the elements of platinum group from the composition of the W-glass. The reagents of waste components were calcined at 650°C for 2 h. These glasses were melted at 1200°C for 2 h in an electric furnace and annealed at 700°C for 1000 h in alumina crucibles in air.

The devitrified glasses were subjected to X-ray powder diffractometry to identify crystals grown in their glasses. An electron-probe microanalyzer was used to determine the elements of the segregated materials.

Results

The annealed W-glass was liable to break. Figure 1-10 and 11 show photographs of the W-glass and the R-glass respectively after annealing at 700°C for 1000 h. In the W-glass, fine segregated materials (Fig. 1-10) were distributed all over the whole body. The phenomenon is presumed to show the distribution of nuclei of platinum group elements. Large clusters of dendroid segregated materials grew in the R-glass. Elements of a dendroid

material in Fig. 1-11 were determined by the use of an electron-probe microanalyzer using an energy-dispersive X-ray analytical system. It was confirmed that the trunk of this material had molybdenum-rich composition and rare-earth elements deposited densely on knots (Fig. 1-12).

The pattern of X-ray powder diffractometry showed that various crystals grew in the glasses. Analysis of these pattern are in progress. The devitrified W-glass will have to be subjected to leaching tests in future.

Acknowledgement

We are indebted to Mr. H. Hidaka of Hitachi Ltd. who took photographs with an electron miscoscope (X-650; SEM).

References

1) G.E. Rindon and J.L. Rhoads, "The colors of Platinum, Palladium and Rhodium in Simple Glasses," J. Am. Ceram. Soc., 39 (5) 173-180 (1956)
2) W.A. Ross et al., Annual Report on the Characterization of High-Level Waste Glasses, PNL-2625 UC-70 (1978)

1.3 Thermal shock resistance

H. Kamizono

It seems that there are three events by which a thermal shock of vitrified high level waste products occurs in storage facilities. The first event is concerned with a decontamination of canisters by water. If outsides of canisters are contaminated and a decontamination by water is done, the surface of vitrified high level waste products is cooled to a water temperature and thermal shocks occur.

The second event is concerned with the cooling system of a storage facility. If the cooling system stops accidentally, the temperature of vitrified high level waste products is raised by decay heats. When the cooling system recovers, vitrified high level waste products suffer from thermal shocks. The third event is related to a fire in storage facilities. If a fire breaks out in a storage facility, a large amount of water may be used to put out the fire. When water used comes into contact with the heated high level waste products, they are quenched to a water temperature and suffer from thermal shocks. The object of this work is to clarify mechanisms of production of fine powder from vitrified waste by the thermal shock at the three events anticipated in a storage facility.

Experimental Procedure

The sample used was a borosilicate glass containing 14% of simulated high level waste. The shape of specimens was a cylindrical rod. They had 25 mm-heights and 25 mm-diameters. The specimen was heated at a given temperature for about 2hrs with a electronic furnace and then dropped into water at a room temperature. The temperature differences between the specimens before dropping and the water were varied from 50°C to 600°C. The specimens after quenching were observed by an optical microscope.

Results

When the temperature difference was 50°C, we could not find any cracks on the surface of specimen with an optical microscope. So the vitrified high level waste products might be good for the 50°C temperature difference.

When the temperature difference became 75°C, several cracks were observed on the surface of specimen, and deterioration of physical properties under the influence of such crack formations might occur. The number of surface cracks increased with the temperature differences in the range of 75°C to 600°C. In this range of temperature differences, it was observed that glass chips which were very small peeled off from the surface of specimens.

Moreover, at the temperature difference of 600°C, the number of cracks greatly increased. After quenching, the specimens were broken into many pieces under a slight impact, and the original cylindrical shape was destroyed. The crack distribution in the specimen was also observed on a fractured surface of specimens at the temperature difference of 600°C. The number of cracks decreases stepwise in the inner part of specimen as shown in Fig. 1-13. This crack distribution might be related to a stress distribution induced in the specimen with quenching. Analysis of relation between the stress and crack distribution is in progress.

As a summary, two critical temperature differences are found through this quenching test. One of them is the 75°C temperature difference at which a crack initiation begins. Another is the 600°C temperature difference at which crack propagations occur markedly and the vitrified products are broken down. These temperature differences may depend on the sample size and shape. The analysis to estimate the crack distribution and production of fine particles is planned by using this experimental results and several calculation models.

Table 1-1 Composition of J-10 waste glass

Oxide form	Calculated (wt%)	Analytical (wt%)	Oxide form	Calculated (wt%)	Analytical (wt%)
SiO_2	38.3	–	CoO	0.09	0.09
B_2O_3	13.0	11.8	NiO	0.50	0.42
Al_2O_3	3.52	7.38	Ag_2O	0.02	–
Na_2O	21.3	20.3	CdO	0.02	–
K_2O	1.14	–	TeO_2	0.17	–
MgO	1.49	0.84	Cs_2O	0.74	0.72
CaO	6.60	6.43	Ce_2O_3	1.13	–
SrO	0.25	0.24	Nd_2O_3	0.73	–
BaO	0.47	0.48	La_2O_3	0.35	–
TiO_2	0.06	0.09	Sm_2O_3	0.31	0.30
P_2O_5	1.32	0.25	Y_2O_3	0.29	0.25
Fe_2O_3	4.33	4.13	Pr_2O_3	0.17	–
MnO_2	0.24	0.22	Dy_2O_3	0.15	0.16
ZrO_2	1.24	1.05	Tb_2O_3	0.04	–
Rb_2O	0.10	–	Er_2O_3	0.03	–
MoO_3	1.31	1.37	Gd_2O_3	0.31	–
Cr_2O_3	0.29	0.20			

Table 1-2 Composition of simulated waste glass

base glass component (%)

SiO_2	52.1
B_2O_3	22.7
Na_2O	11.2

Waste component (%)

(Total 14 %)

Fe_2O_3	2.4	REOx	3.5
Na_2O	2.4	CeO_2	1.13
MoO_3	1.3	Nd_2O_3	0.73
ZrO_2	1.2	La_2O_3	0.35
Cs_2O	0.74	Sm_2O_3	0.31
NiO	0.50	Gd_2O_3	0.29
BaO	0.47	Y_2O_3	0.29
Cr_2O_3	0.39	PrOx	0.17
SrO	0.25	Dy_2O_3	0.15
P_2O_5	0.24	Tb_2O_3	0.04
MnO_2	0.19	Er_2O_3	0.03
TeO_2	0.17		
Rb_2O	0.09		
CoO	0.09		
Ag_2O	0.02		
CdO	0.02		

Table 1-4 Composition of a borosilicate base glass

Component	Content (wt%)	Reagent used
SiO_2	60.56	SiO_2
B_2O_3	26.39	$Na_2B_4O_7$
Na_2O	13.05	$Na_2B_4O_7$, Na_2CO_3
Total	100.00	

Table 1-3 Composition of a simulated HLW

Component	Content(wt%)	Reagent used
RuO_2	5.06	$RuCl_3$
Rh_2O_3	1.05	$Rh(NO_3)_3$
PdO	2.77	$Pd(NO_3)_2$
Ag_2O	0.15	$AgNO_3$
CdO	0.16	$Cd(NO_3)_2\ 4H_2O$
SeO_2	0.11	SeO_2
Rb_2O	0.63	$RbNO_3$
SrO	1.76	$Sr(NO_3)_2$
ZrO_2	8.53	$ZrO(NO_3)_2\ 2H_2O$
MoO_3	9.00	$H_2MoO_4\ H_2O$
MnO_2	1.34	$Mn(NO_3)_2\ 6H_2O$
SnO_2	0.10	$SnCl_4\ xH_2O$
Sb_2O_3	0.03	$SbCl_3$
TeO_2	1.18	TeO_2
Cs_2O	5.07	$CsNO_3$
BaO	3.24	$Ba(NO_3)_2$
La_2O_3	2.63	$La(NO_3)_3\ 6H_2O$
CeO_2	7.03	$Ce(NO_3)_3\ 6H_2O$
Pr_6O_{11}	2.57	$Pr(NO_3)_3\ 6H_2O$
Nd_2O_3	8.56	$Nd(NO_3)_3\ 6H_2O$
Sm_2O_3	1.70	$Sm(NO_3)_3\ 6H_2O$
Eu_2O_3	0.32	$Eu(NO_3)_3\ 6H_2O$
Gd_2O_3	0.20	$Gd(NO_3)_3\ 6H_2O$
Y_2O_3	1.04	$Y(NO_3)_3\ 6H_2O$
Na_2O	16.52	$NaNO_3$
P_2O_5	1.67	H_3PO_4
Fe_2O_3	13.83	$Fe(NO_3)_3\ 9H_2O$
Cr_2O_3	2.01	$Cr(NO_3)_3\ 9H_2O$
NiO	1.74	$Ni(NO_3)_2\ 6H_2O$
Total	100.00	

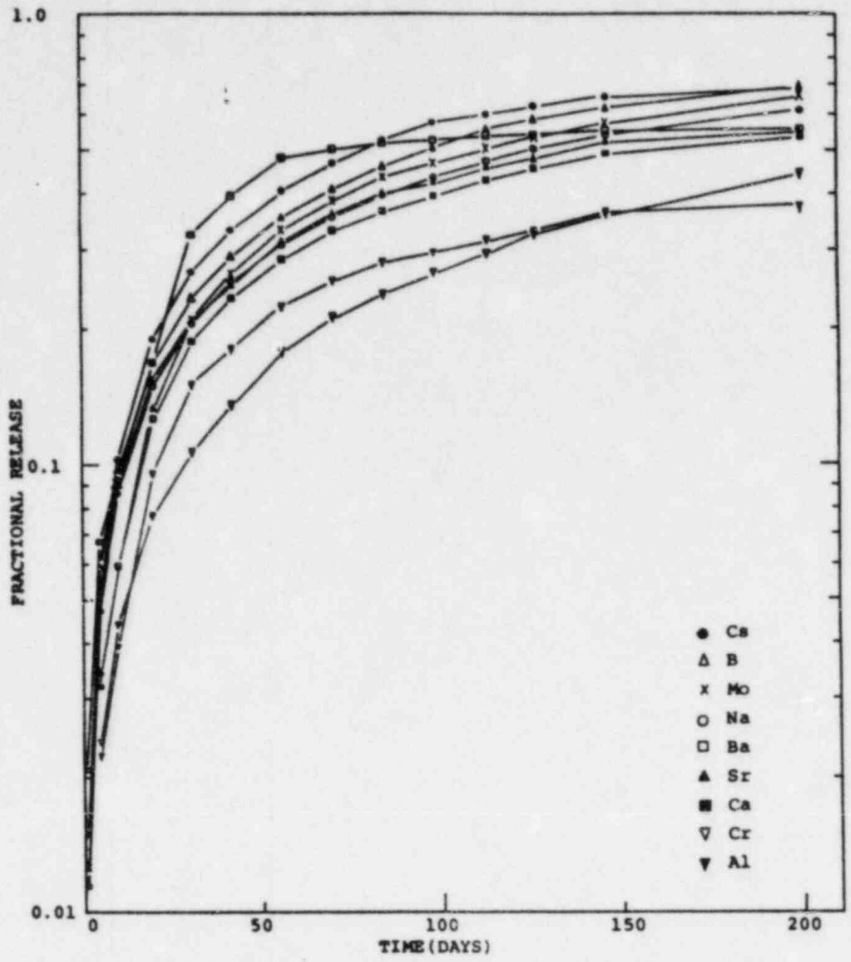

Fig.1-1 Time Dependence of Fractional Releases for detectable Elements (Fe, and Ce are under detection limit of ICP)

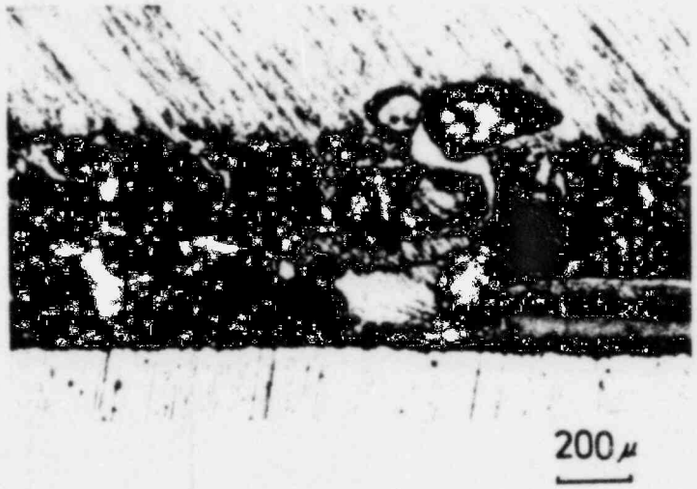

Fig1-2 Microphotograph of surface layer

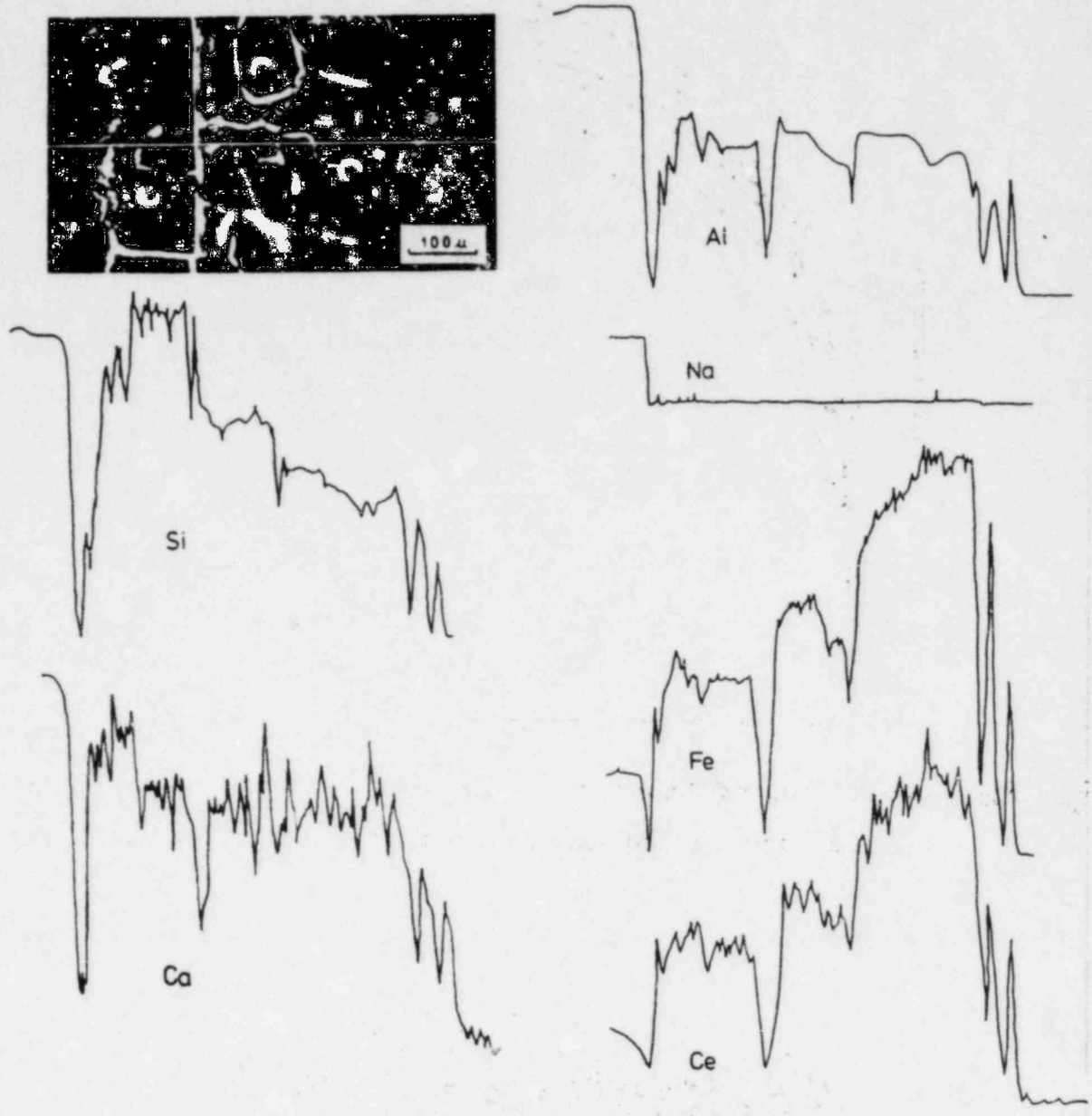

Fig.1-3 X-ray fine scans of surface layer of waste glass

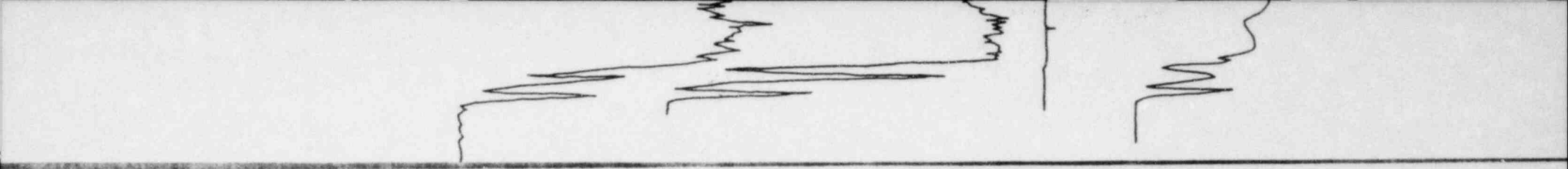

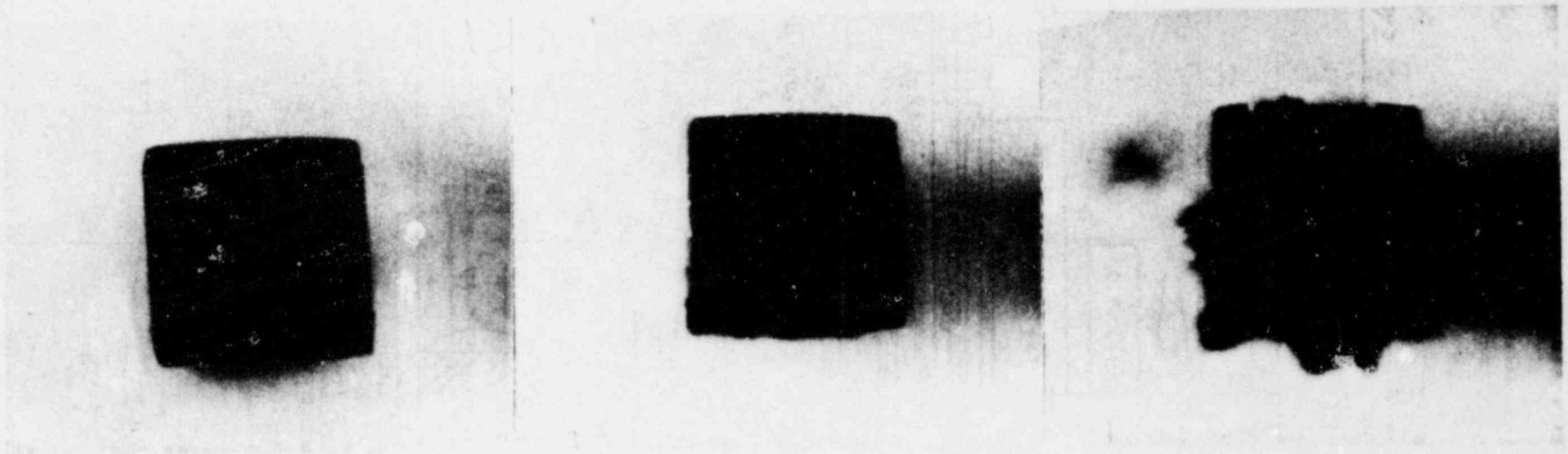

Fig.1-4 Photograph of simulated waste glasses after leaching test

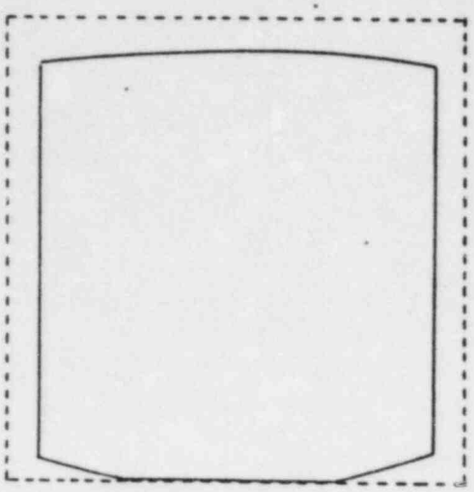

Fig.1-5 Shape of glass sample leached at 100°C for 18 days.
(--- Non leached,
—— leached)

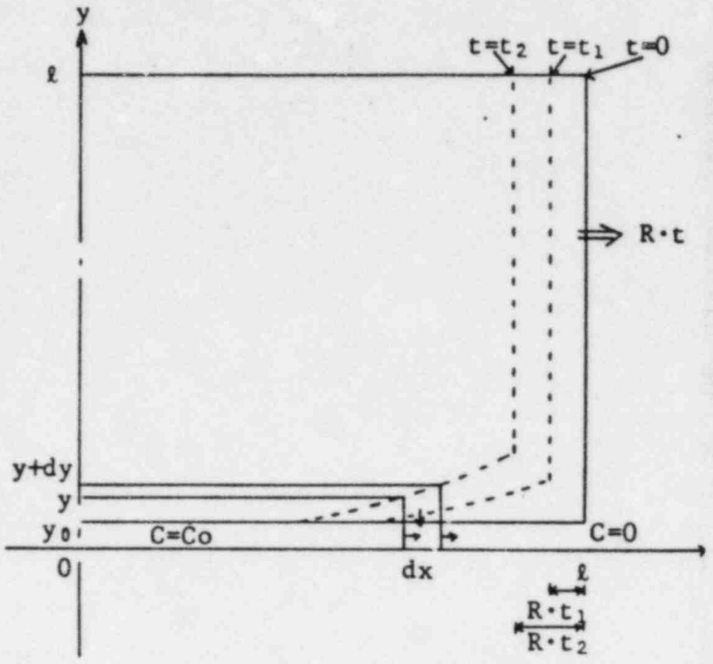

Fig.1-6 Model of Glass Leaching

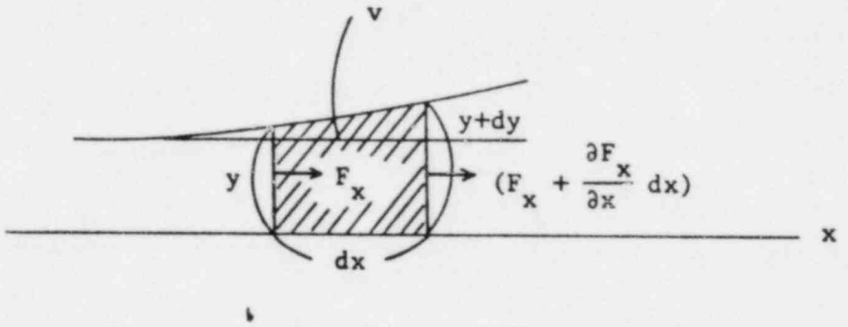

Fig.1-7 Element of volume

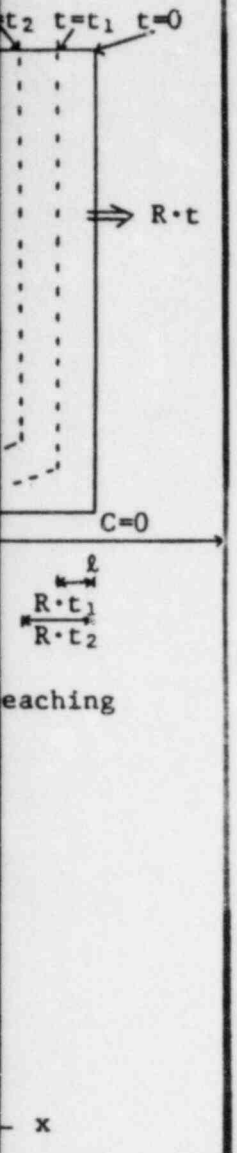

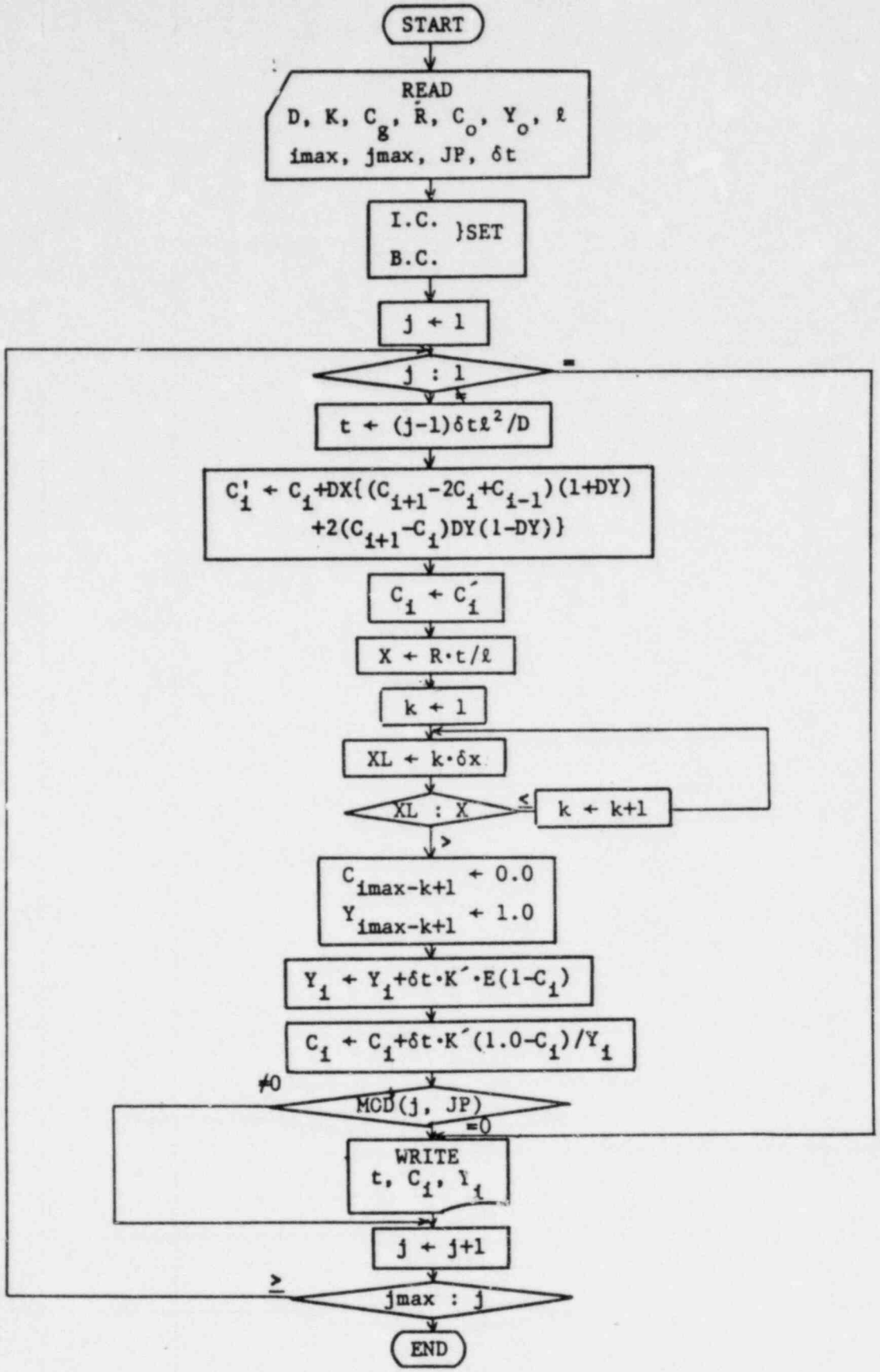

Fig.1-8 Flow Sheet of the Program

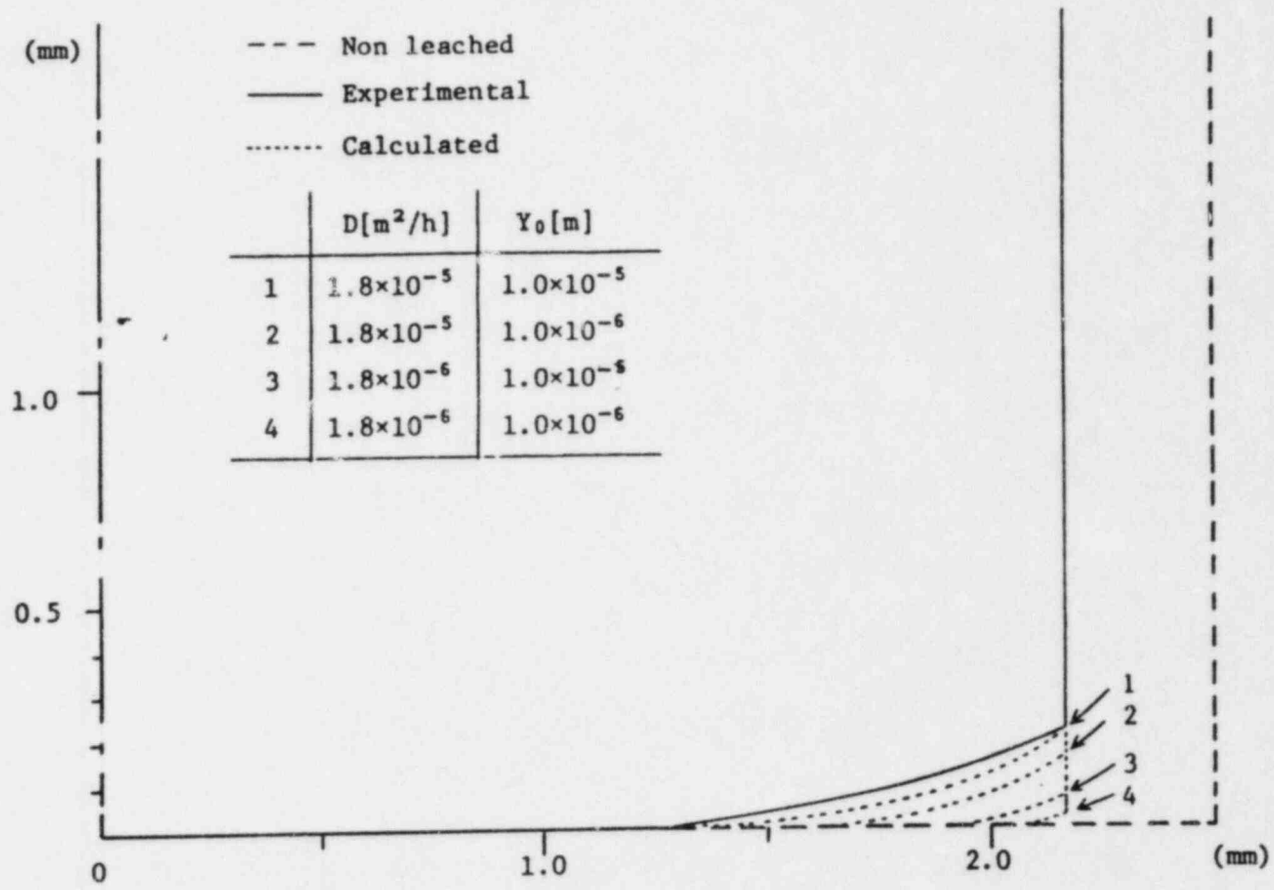

	D[m²/h]	Y_0[m]
1	1.8×10^{-5}	1.0×10^{-5}
2	1.8×10^{-5}	1.0×10^{-6}
3	1.8×10^{-6}	1.0×10^{-5}
4	1.8×10^{-6}	1.0×10^{-6}

Fig.1-9 Comparison between experimental result and calculated results

JAERI-M 82-140

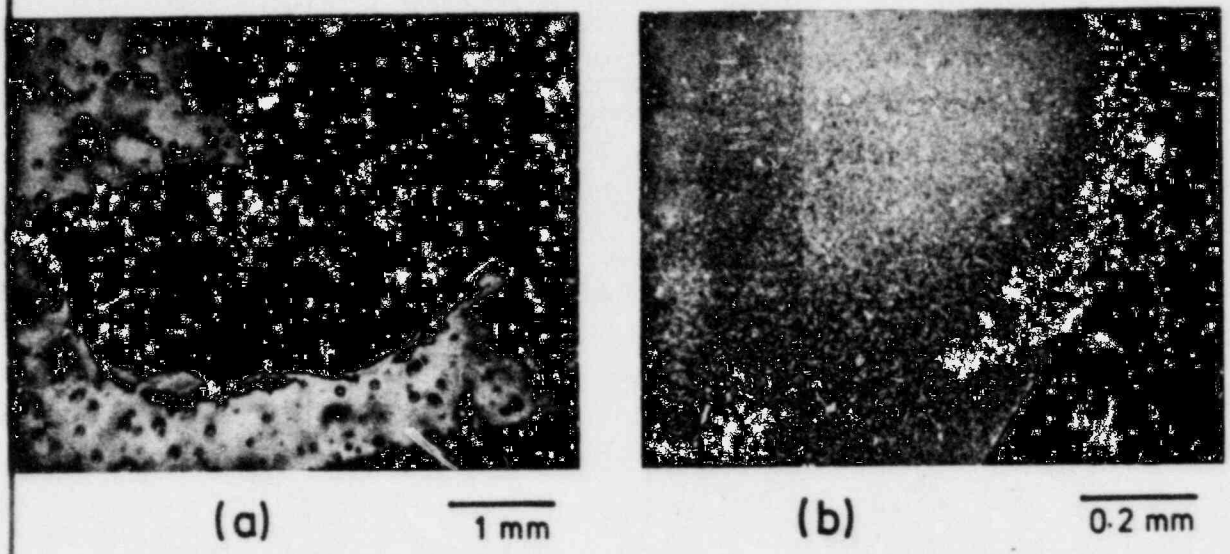

Fig. 1-10 Microphotograph of the W-glass after annealing at 700 °C for 1000 h

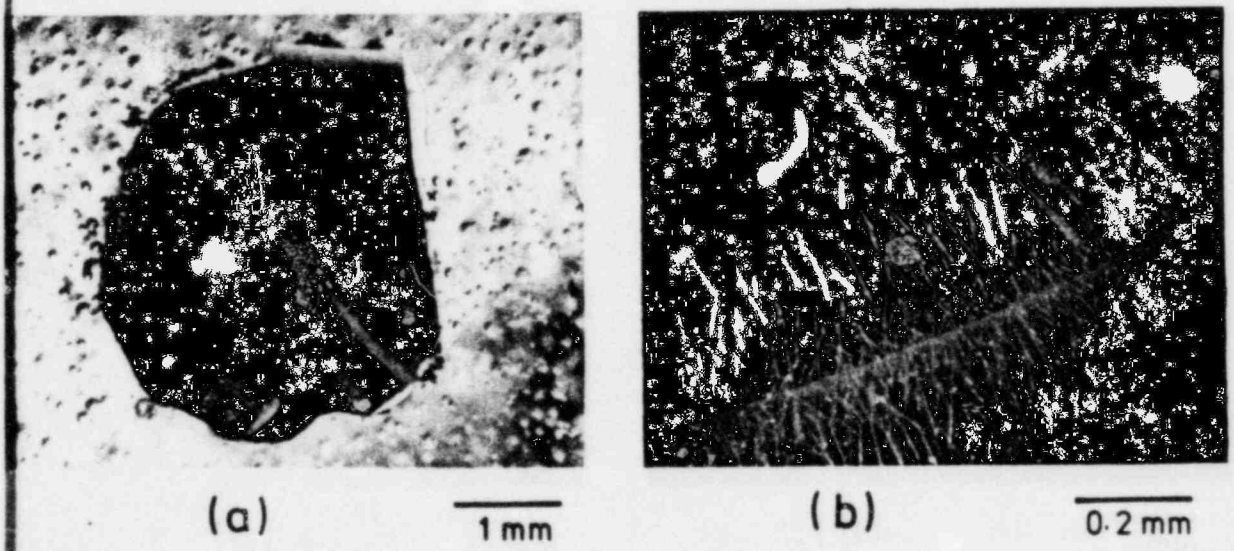

Fig. 1-11 Microphotograph of the R-glass after annealing at 700 °C for 1000 h

Fig.1-9 Comparison between experimental result and calculated results

SEM Image

0.01 mm

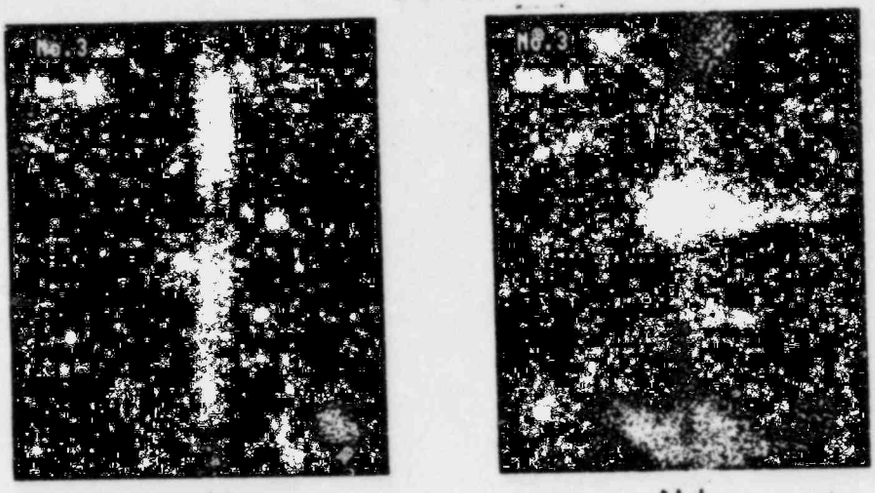

Mo Nd

Fig. 1-12 Microprobe X-ray maps, R-glass (devitrified at 700 °C for 1000 h)

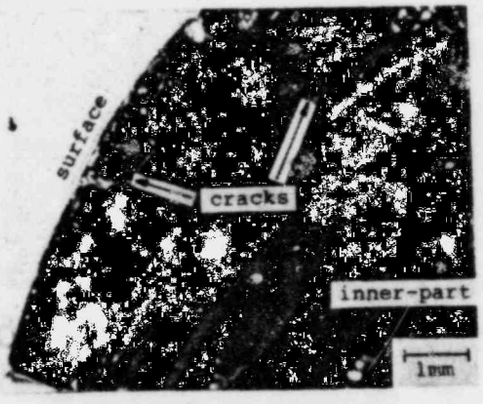

Fig.1-13 Fractured surface of a simulated high level waste product.

Temperature difference = 600°C.

2. Development of Alternative HLW form

Syntheses of SYNROC and distribution of radwaste elements over its constituent minerals

T. Murakami

SYNROC (Synthetic Rock) has been proposed for immobilization of high-level waste (HLW) by Ringwood[1), 2)]. SYNROC consists of three minerals: hollandite, $BaAl_2Ti_6O_{16}$; perovskite, $CaTiO_3$; and zirconolite, $CaZrTi_2O_7$. Of radwaste elements, Cs and Sr, from which decay heat mainly generates, preferentially enter hollandite and perovskite, respectively, and long half-life actinides, zirconolite. Although leaching behavior and radiation damage of SYNROC have been intensively investigated (see, for example, references 3, 4, 5 and 6), distribution of radwaste elements, which may be affected by compositions, forming temperatures, etc., has not been fully studied. We have made a study of SYNROC especially emphasized on distribution of radwaste elements over the constituent minerals.

Experimental

Experiments were carried out as follows: stage 1; the above three minerals, $BaAl_2Ti_6O_{16}$, $CaTiO_3$ and $CaZrTi_2O_7$ were synthesized, stage 2; each constituent mineral was synthesized containing one of simulated HLW elements, and stage 3; SYNROC containing 10 wt% simulated HLW (Table 2-1) was synthesized. Stage 1 and 2 were carried out to identify mineral phases of SYNROC and to confirm the accommodation of the elements in each mineral. We also examined effect of fabrication condition on density and crystallinity at stage 2. Stage 3 was made for examination of distribution of simulated HLW elements.

Composition. Compositions at each stage are given in Table 2-2.

Fabrication. Fabrication procedure was as follows:

1) some of TiO_2, Al_2O_3, ZrO_2, Ca-, Ba-nitrates and simulated

waste were mixed by ballmilling with alcohol media. 2) The mixture was calcined at 1000°C for about 10 hours and then re-milled. 3) The milled powder was subjected to one of the three methods: atomospheric sintering after cold-pressing (1290°C for 15 to 25 hours, 580 kg/cm²); hot-pressing (1200°C and 600 kg/cm² for 2 hours); and atomospheric sintering after hot-pressing (1290°C for 25 hours, 1200°C and 600 kg/cm² for 2 hours). And finally the pelletlike specimen was obtained.

Analysis. X-ray diffraction method was used for identification of mineral phases and for confirming accommodation of simulated HLW elements by shift of diffraction peaks and/or absense of unreactants at stage 2. A powder specimen at stage 3 was supplied for examination of distribution of simulated HLW elements by means of analytical electron microscopy (H-600 with Kevex EDX system; Hitachi Ltd.).

Results and discussion

Cs and Sr were properly accommodated in hollandite and perovskite, respectively, which contained large amount of Cs_2O and SrO, respectively (Table 2-2, see stage 2). In the system La_2O_3-TiO_2-CaO-ZrO_2, where 25.1 wt% La_2O_3 was contained, there formed perovskite and zirconolite. When the amount of La_2O_3 was decreased to 2.8 wt% in the above system, only zirconolite formed. Accordingly, accommodation of La, which is considered to simulate actinides, is limited in the zirconolite phases, though solubility limit of actinides themselves remains unravelled.

Density was the highest when specimens were synthesized using hot-pressing (Table 2-2). Crystallinity was high when specimens were synthesized using atomospheric sintering but these specimens had rather low density (Table 2-2). Sepecimens by atomospheric sintering after hot-pressing had high density and crystallinity. Appropriate fabrication conditions should be selected after examining leaching behavior

of specimens by different conditions.

Distribution of simulated HLW elements over the constitutent minerals is given in Table 2-3. Mineral phases in SYNROC were distinguished on the basis of the X-ray intensity images by analytical electron microscope, for example, zirconolite, by high Zr concentration. Cs was found in hollandite as predicted[2], which indicated appropriate accommodation of most amount of initial Cs. Na occurred only in preovskite and this result didn't agree with that by Ryerson et al.[7] who reported Na occurred in all three mineral phases. Rare earth elements such as La, Ce, Nd might be accommodated in both perovskite and zirconolite. Fe occurred in all three phases while it was considered to occur in hollandite and/or in metallic state[2), 7)]. Mo was also considered to be found in hollandite and/or in metallic stage but our result showed Mo occurred only in perovskite. Since Cs was accommodated in hollandite and Mo, in perovskite, water-soluble Cs-molybdates might not occur. It must be indispensable to examine all of the radwaste elements are really accommodated in appropriate host phases.

References

1) Ringwood, A.E., "Safe disposal of high-level nuclear wastes: a new strategy", Australian National University Press, Canberra (1978).

2) Ringwood, A.E., Kesson, S.E., Ware, N.G., Hibberson, W.D. and Major, A., Geoch. J., 13, 141 (1979).

3) Coles, D.G. and Bazan, F., Nucl. Tech., 56, 226 (1982).

4) Kennedy, C.R., Flynn, K.F., Arons, R.M. and Dusek, J.T., Nucl. Tech., 56, 278 (1982).

5) Oversby, V.M. and Ringwood, A.M., Rad. Was. Man, 1, 289 (1981).

6) Ringwood, A.E., Overby, V.M. and Sinclair, W., "Scientific Basis for Nuclear Waste Management 2, 273 (1980).

7) Ryerson, F. J., Hoenig, C.L. and Smith, G.S., UCRL-86880 (1981).

Table 2-1 Composition of JW-8 simulated HLW.

Oxide form	M_w	Oxide Reagents used	g/l
$1/2Rb_2O$	93.468	0.6338	0.735
SrO	103.62	0.4896	1.968
ZrO_2	123.22	0.4610	9.544
MoO_3	143.94	0.7998	10.077
MnO_2	86.938	0.3029	1.496
$1/2Fe_2O_3$	79.847	0.1976	3.399
CoO	74.933	0.2575	0.693
NiO	74.7	0.2569	1.891
$1/2Ag_2O$	115.868	0.6821	0.171
CdO	128.4	0.5431	0.179
TeO_2	159.6	1.00	1.320
$1/2Cs_2O$	140.905	0.7229	5.675
BaO	153.3	0.5867	3.631
$1/2Na_2O$	30.99	0.3646	18.485
$1/2P_2O_5$	70.974	0.7242	1.868
$1/2Fe_2O_3$	79.847	15.492	15.492
$1/2Cr_2O_3$	75.996	2.241	2.241
NiO	74.7	1.950	1.950
$1/2RE_2O_3$	168.24	27.223	27.223
Total			108.038

Table 2-3 Distribution of HLW elements by means of AEM*)

	Ti	Al	Ca	Zr	Ba	Na	Cs	Sr	La	Ce	Nd	Fe	Ni	Mn	Mo	Si	P
Hollandite	M	M	T	-	M	-	+	-	-	-	-	+	+	+	-	-	-
Perovskite	M	T	M	-	-	+	-	+	+	+	+	+	-	-	+	+	+
Zirconolite	M	T	M	M	T	-	-	-	+	+	+	+	-	-	-	+	-

M: major, T: trace, +: present, -: not detect

*) Elements not presented in this table are below detection limit

Table 2-2 Compositions and other details of synthesized minerals

Stage	Specimen number	Composition (Wt%) TiO_2	Al_2O_3	ZrO_2	CaO	BaO	Cs_2O	SrO	La_2O_3	JW-B[1]	Fabrication[2]	Phase[3]	Density (g/cm^3)	Crystallinity[4]
1	800710	65.3	13.9	-	-	20.9	-	-	-	-	A	H	-	-
	801005	58.8	-	-	41.3	-	-	-	-	-	A	P	-	-
	800714	47.1	-	36.3	16.5	-	-	-	-	-	A	Z	-	-
2	801006	60.0	12.8	-	-	9.6	17.6	-	-	-	A	H	2.7	6
	810204	60.0	12.8	-	-	9.6	17.6	-	-	-	B	H	4.2	2
	810204b	60.0	12.8	-	-	9.6	17.6	-	-	-	C	H	3.4	10
	801014	56.8	-	-	35.9	-	-	7.4	-	-	A	P	3.2	5
	810121	56.8	-	-	35.9	-	-	7.4	-	-	B	P	4.0	5
	810121b	56.8	-	-	35.9	-	-	7.4	-	-	C	P	3.9	10
	801008	41.1	-	19.3	14.4	-	-	-	25.1	-	A	P, Z	4.4	8
	810122	41.4	-	19.3	14.4	-	-	-	25.1	-	B	P, Z	4.8	5
	810122b	41.1	-	19.3	14.4	-	-	-	25.1	-	C	P, Z	4.1	10
3	810907	54.9	6.5	10.9	10.9	6.9	-	-	-	10.0	C	H,P,Z	-	-

1) See Table 2. 2) A: atomospheric sintering after cold-pressing, B: hot-pressing, C: atomospheric sintering after hot-pressing. 3) H: Hollandite, P: Perovskite, Z: Zirconolite Only major phasesare shown.

4) Crystallinity was roughly obtained from height of a major peak.

3. Durability tests with γ-ray irradiation of structural materials for HLW storage facility

3.1 Concrete

S. Muraoka

As a part of safety evaluation of high level waste for interim air cooling storage system, the effect of γ-ray irradiation on concrete material has been studied.

The most important property of the material in the storage is a structural integrity. In the present study, the same procedure was followed on both the irradiated and non-irradiated sample to detect the changes of physical and mechanical properties.

Experimental

(1) Sample preparation

The composition of the cement is shown in Table 3-1. Concrete samples are made with mixing of cement, aggregate, water and water reducing agent. The dimension of each material and the mixing ratio is shown in Table 3-2. The size of concrete specimen is 10 cm diameter and 20 cm long.

(2) Measurement of physical and mechanical properties

The following measurements were made on both irradiated and non-irradiated samples:

1) Weight
2) Compressible strength
3) Young's modulus
4) Poison ratio
5) Dimension

(3) Irradiation test

The specimens were exposed to γ-ray of max 5.22×10^8 Röntgen at 100°C. For the comparison the tests without γ-ray exposure were carried out at 20°C and 100°C.

Results

According to the irradiation test at 100°C, there were no differences between the measured properties of γ-ray irradiated specimens to the dose of 5.22×10^8 R and non-irradiated specimens. The irradiation effect on neutralization was slightly found as shown in Fig. 3-1. On the other hand, it was clarified that the effect of temperature of circumstance was larger than that of γ-irradiation on the physical and mechanical properties. Measured properties, such as compressible strength showed a decrease of a few percent to about 30% at 100°C as compared with at 20°C. The difference are shown typically in Fig. 3-2. In this figure, A and B shows the storage periods 300 hours and 600 hours respectively.

This work was carried out in cooperation by JAERI and Sumitomo Cement Co. Ltd.

3.2 Corrosion resistance of alloys[1)]

T. Furuya

Introduction

Canisters for high-level solidified waste (HLW) and materials used as their packages and their storage facilities are exposed with γ-ray. The candidate materials are austenitic stainless steels and nickel base alloys. These alloys retain a great deal of their resistance to general corrosion and are widely used as industrial materials. But their corrosion resistance under γ-ray irradiation have not been known well although many workers have studied[2 ∿ 8)] till now.

The effects of γ-ray irradiation on stress corrosion cracking (SCC) have been studied about the candidate alloys for HLW canisters, overpackages and storage facility materials.

This study was carried out in cooperation by JAERI and Kobe Steel Ltd.

Experimental

(1) Alloy materials and specimen form

In this report, the alloy materials tested were Type 304 SS, Type 304L SS, Type 304EL SS, Type 309S SS, Incoloy 825, Inconel 600, Inconel 625 and SMA 50. In order to sensitize them, they were heat-treated for 100 min at 700°C and for 24hr at 500°C. Incoloy, Inconels and Type 309S SS were heated for 30 min at 1100°C before the treatment. Double U-bend type secimens were used as shown in Fig. 3-3.

(2) γ-ray irradiation

Two tests were carried out under the dose rate of 1.1×10^5R/hr with Co-60. At the first test (test 1), corrosion test specimens were immersed in boiling deionized water on the assumption of water cooling system as interim storage of HLW. The apparatuses are schematically shown in Fig.3-4. In the first test, the water supply system caused to introduce chloride ion and oxygen gas to testing water. At the second

test (test 2), glass apparatus shown in Fig. 3-5. was used. The samples were limited to Type 304 SS and Type 304 EL SS. On the other hand, corrosion test in dry atmosphere was carried out by placing the specimens in air atmosphere at room temperature on the assumption of air cooling system. The other conditions were similar to the above tests.

(3) Analyses of SCC failures

Susceptibilities to SCC failures were evaluated by measuring maximum depth and numbers of SCC with an optical metallography. SCC fractures were observed with a scanning electron microscope and an optical metallography in order to research metallurgically.

Results

(1) Tests of SCC in boiling deionized water

Maximum depths of SCC failures in the first and second test are given in Table 3-3 and 3-4, respectively.

As shown in Table 1, sensitized Type 304 SS, Type 304L SS and Type 309S SS were susceptible to SCC in boiling deionized water under γ-ray irradiation, but the others were immune to SCC although SMA 50 rusted over its surface. The failures on inner specimens were observed more than on outer ones.

In the first test, chloride ion concentrations in the testing water were analyzed. Chloride ion were 0.2 ppm to 3.8 ppm in the testing water. Since its concentration in deionized water (relative resistance $> 5 \times 10^6 \Omega \cdot cm$) was usually less than 0.1 ppm, chloride ion in auxiliary water from chloride compounds in air atmosphere would enter to testing water in this test.

As shown in Table 3-4 (second test), SCC failures were found only on the inner specimens of Type 304 SS under γ-ray irradiation. And the maximum depth of SCC failures on sensitized Type 304 SS increased with irradiated period as shown in Fig. 3-6. In the second test, chloride ion concentrations

in the testing water were less than 0.7 ppm.

SCC failures of sensitized Type 304 SS, Type 304L SS and Type 309S SS were observed by an optical metallography. SCC failures of sensitized Type 304 SS were shown in Fig. 3-7. These SCC failures were observed with a scanning electron microscope. As shown in Fig. 3-8, all these SCC failures were intergranular cracking modes and there were no differences between irradiated specimens and non irradiated ones. And then, cross sections of each specimens were observed with an optical metalography as shown in Fig. 3-9. As shown in photographs, there were no diffrences between irradiated specimens and non irradiated ones.

(2) Test of SCC in air atmosphere at room temperature

All these alloys were not susceptible to SCC in air atmosphere at room temperature with and without γ-ray irradiation, but SMA50 rusted over its surface.

Discussions

(1) Effects of γ-ray irradiation

SCC failures of Type 304 SS, Type 304L SS and Type 309S SS were found in boiling deionized water under both γ-ray irradiation and non irradiation in first test, but, in second test, SCC failures of Type 304 SS were found only under γ-ray irradiation. Many workers[9)~13)] showed that the presences of grain boundaries impoverished chromium, high tension stress, dissolved oxygen and chloride ion caused alloy materials to be susceptible to SCC, but only the presence of chloride ion did not cause to be susceptible to SCC. Therefore, our results showed that in first test chloride ion and dissolved oxygen from auxiliary water would mainly cause to be susceptible to SCC, but, in second test, radiolysis of water under γ-ray irradiation would mainly cause to be susceptible to SCC. And it was reported[14)] that oxidant such as, O_2, O_2^- and HO_2^- etc. were generated by radiolysis of

water. The content of these products must be high in this space between outer and inner specimen. This would be the reason why SCC failures arose on inner specimen (see Table 3-3 and 3-4).

(2) Effects of alloy materials

Type 304 EL SS of low carbon content were not susceptible to SCC. Therefore, these SCC failures were due to grain boundaries impoverished in chromium by chromium carbide precipitation.

Incoloy 825 and Inconel 625 were not susceptible to SCC in this test. This would be due to containing carbide formers to render them insensitive to intergranular crackings such as Ti and Nb.

It was reported that Ni content of alloys made chromium carbide to disperse.[15),16)] Therefore, non-SCC failures of Inconel 600 would be due to re-dispersion of chromium carbide by high Ni content.

References

1) T. Furuya, S. Muraoka, S. Tashiro, K. Araki, H. Tomari, K. Fujiwara and T. Fukuzuka: JAERI-M 82-061.
2) S. Ohno and K. Furukawa: Genshiryoku Kogyo 20 4 ('74)
3) A.V. Byalobzheskii (translated by Aladjem): Israel Program for Scientific Translation Ltd. ('70) (translated from Russian).
4) J.W. Braithwaite and M.A. Molecke: Nuclear and Chemical Waste Management, 1, 1 ('80)
5) W.N. Rankin: DP-MS-80-47 ('80)
6) N. Fujita, M. Akiyama and T. Tamura: Corrosion NACE, 37, 6 ('81)
7) M. Muroi, N. Fujita and M. Akiyama: Annual Meeting of the Atomic Energy Society of Japan ('81) C.7.
8) M. Kuribayashi and H. Okabayashi: Annual Meeting of the Japan institute of metals ('81) 471
9) F.P. Ford and M.J. Prvich: Corrosion, 35, 569 ('79)

10) M.E. Indig and A.R. McIllee: Paper presented to NACE corrosion/78, paper No.190.

11) Sugimoto, Maekawa, Kagawa: Boshoku Gijutsu, 14 4 p.11 ('65)

12) M. Kowaka: Iron and Steel, 60 3 p.105 ('74)

13) Shimizu: Genshiryoku-Kogyo, 21 7 p.19 ('76)

14) O. Allen: "The Radiation Chemistry of Water and Aqueous Solution", D. Van Nostrand ('61)

15) T. Fukuzuka, K. Shimogori, K. Fujiwara and H. Tomari: Proceedings, Seminar on Countermeasures for Pipe Cracking in BWRs, paper NO.46, EPRI, WS-79-174, Workshop Report ('80)

16) Namada, Maruyama, Nakao and Yamasaki: Meeting of Japan Society of Corrosion Engineering, p.200 ('79)

Table 3-1 Chemical composition of normal Portland cement

Type	Ignition Loss	Non Soluble Balance	SiO_2	Al_2O_3	Fe_2O_3	CaO	MgO	SO_3	Total (%)
Normal Portland Cement	0.5	0.1	22.2	5.9	2.8	64.3	1.4	2.0	99.2
Cement (JIS R5210)	<3.0						<5.0	<3.0	

Type	Hydraulic Modulus	Silica Modulus	Iron Modulus	Activity Index
Normal Portland Cement	2.04	2.6	2.1	3.8
Cement (JIS R5210)				

Table 3-2 Dimension of each material and mix proportion

Coarse aggregate (max.)	20 mm	Unit weight (kg/m^3)	2288
Slump	10.2 cm	Water	175
Air	4.3 %	Cement	318
Water/cement ratio	55.0 %	Fine aggregate	783
Fine aggregate	44.0 %	Coarse aggregate	1012
Unit weight	2288 kg/m^3		

Table 3-3 SCC test in boiling deionized water (First test)

[Dose rate ; 1.1×10^5 R/hr
Specimen numbers for each test ; 2]

Alloy	Time (day)	γ-ray irradiation: Total dose (R)	γ-ray irradiation: Max. depth of SCC (mm) Plain	γ-ray irradiation: Max. depth of SCC (mm) V-notched	Non irradiation: Max. depth of SCC (mm) Plain	Non irradiation: Max. depth of SCC (mm) V-notched
Type 304 ss	7	2.0×10^7	1.5*1/0, 0.7*2/0	1.8/0 , 1.8/0	1.3/0 , 0.6/0	>1.5/0 , 1.3/0
	14	4.0×10^7	>2/0 , >2/0	>2*3/0 , >2/0	>2/0 , >2/0	>1.5/0 , >1.5/0
	30	8.6×10^7	>2/0 , >2/0	>2/0 , >2/0	>2/0 , >2/0	>2/0 , >2/0
	60	1.7×10^8	>2/0 , >2/0	>2/0 , >2/>1.5*4	>2/0 , >2/0	>2/0 , >2/0
	90	2.6×10^8	>2/0 , >2/0	>2/>1.5, >2/0	>2/0 , >2/0	>1.5/>1.5, >1.5/>1.5
	180	5.2×10^8	>2/0 , >2/0	>2/>1.5, >2/>1.5	>2/0 , >2/0	>1.5/>1.5, >1.5/0
Type 304L ss	180	5.2×10^8	>2/0 , >2/0	>2/>1.5, >2/>1.5	>2/0 , >2/0	>1.5/>1.5, >1.5/0
	7	2.0×10^7	0/0 , 0/0	0/0 , 0/0	0/0 , 0/0	0/0 , 0/0
	14	4.0×10^7	0/0 , 0/0	0/0 , 0/0	0/0 , 0/0	0/0 , 0/0
Type 304EL ss	30	8.6×10^7	0/0 , 0/0	0/0 , 0/0	0/0 , 0/0	0/0 , 0/0
	60	1.7×10^8	0/0 , 0/0	0/0 , 0/0	0/0 , 0/0	0/0 , 0/0
	90	2.6×10^8	0/0 , 0/0	0/0 , 0/0	0/0 , 0/0	0/0 , 0/0
	180	5.2×10^8	0/0 , 0/0	0/0 , 0/0	0/0 , 0/0	0/0 , 0/0
Type 309S ss	180	5.2×10^8	>2/0 , >2/0	— , —	>2/0 , 0/0	— , —
Incoloy 825	180	5.2×10^8	0/0 , 0/0	0/0 , 0/0	0/0 , 0/0	0/0 , 0/0
Inconel 600	180	5.2×10^8	0/0 , 0/0	0/0 , 0/0	0/0 , 0/0	0/0 , 0/0
Inconel 625	180	5.2×10^8	0/0 , 0/0	0/0 , 0/0	0/0 , 0/0	0/0 , 0/0
SMA 50	180	5.2×10^8	0/0 , 0/0*5	— , —	0/0 , 0/0*5	— , —

*1 ; Max. depth of SCC on inner specimen
*2 ; Max. depth of SCC on outer specimen
*3 ; >2 : failed from other than V-notched root
*4 ; >1.5 : failed from V-notched root
*5 ; Pitting corrosion was observed

Table 3-4 SCC test in boiling deionized water (Second test)

[Dose rate ; 1.1×10^5 R/hr
Specimen numbers for each test ; 2]

Alloy	Time (day)	γ-ray irradiation: Total dose (R)	γ-ray irradiation: Max.depth of SCC (mm) Plain	γ-ray irradiation: Max.depth of SCC (mm) V-notched	Non irradiation: Max.depth of SCC (mm) Plain	Non irradiation: Max.depth of SCC (mm) V-notched
Type 304 ss	7	2.0×10^7	0.8*/0 , 1.1**/0	—	0/0 , 0/0	—
	14	4.0×10^7	1.5/0 , 1.3/0	—	0/0 , 0/0	—
	30	8.6×10^7	1.8/0 , 1.9/0	—	0/0 , 0/0	—
	60	1.7×10^8	>2/0 , >2/0	>1.5***/>1.5, >1.5/>1.5	0/0 , 0/0	0/0 , 0/0
Type 304EL ss	7	2.0×10^7	0/0 , 0/0	—	0/0 , 0/0	—
	14	4.0×10^7	0/0 , 0/0	—	0/0 , 0/0	—
	30	8.6×10^7	0/0 , 0/0	—	0/0 , 0/0	—
	60	1.7×10^8	0/0 , 0/0	—	0/0 , 0/0	—

* ; Max. depth of SCC on inner specimen.

** ; Max. depth of SCC on outer specimen.

*** ; >1.5 : failed from V-notched root.

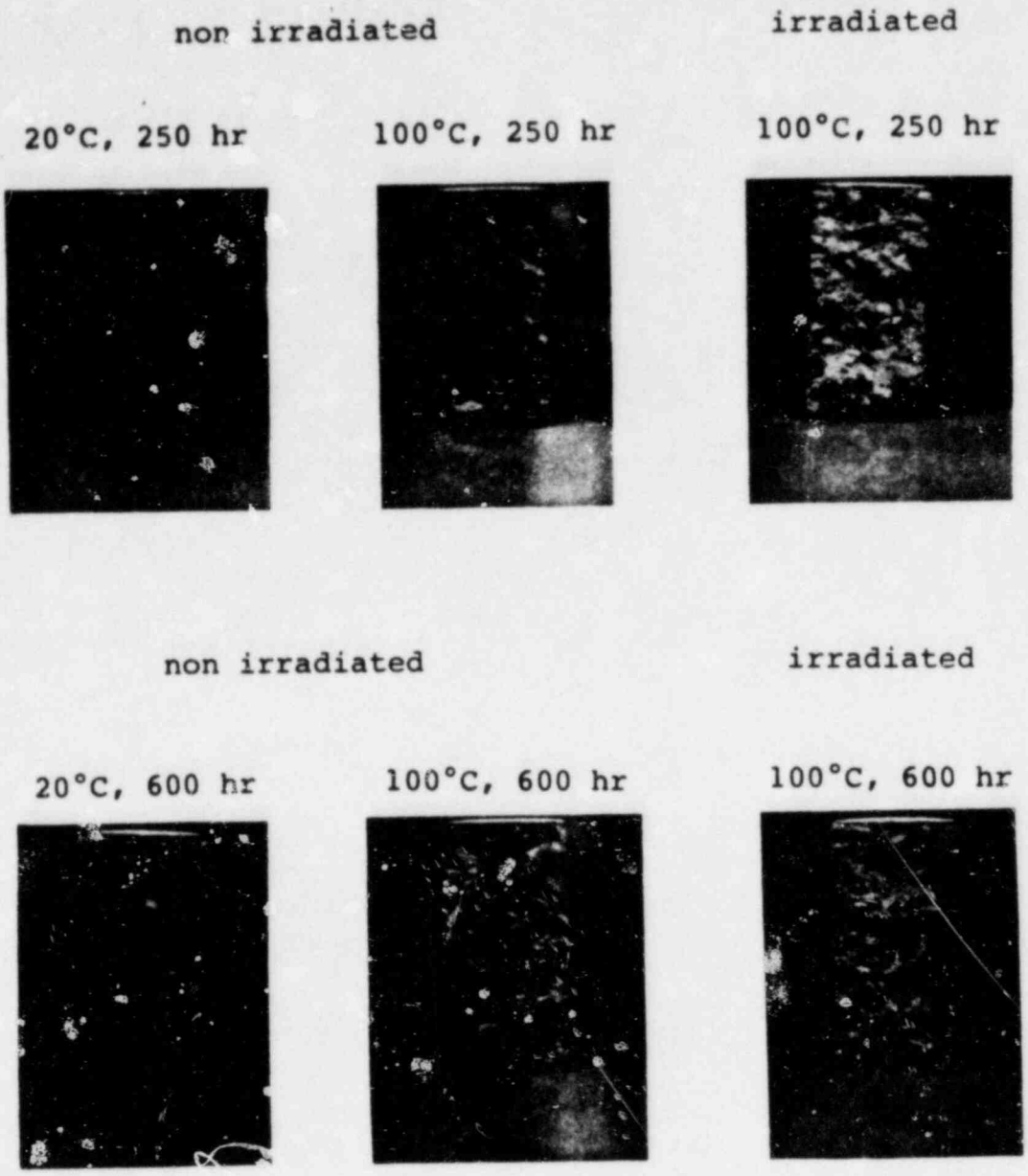

Fig. 3-1 Irradiation effect on neutralization of concrete

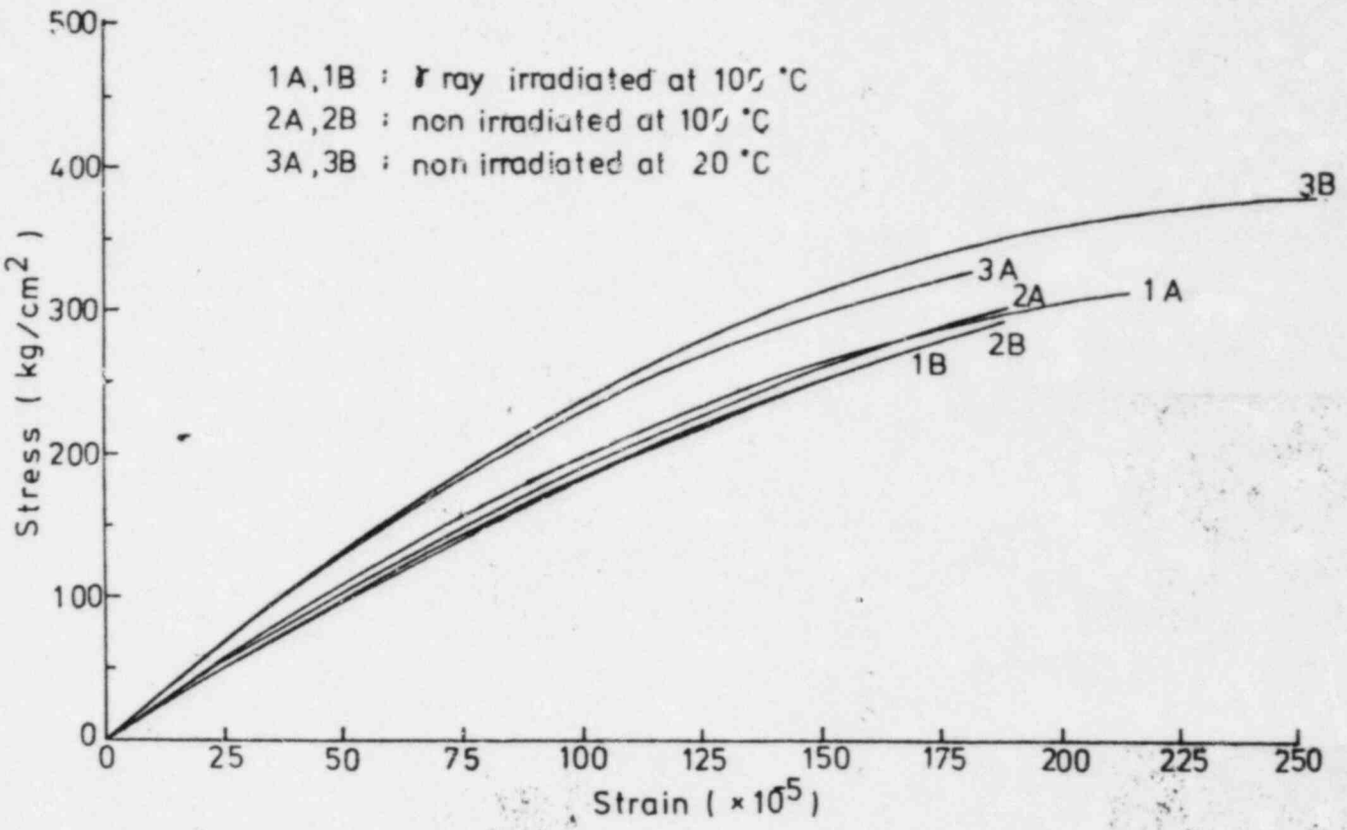

Fig. 3-2 Stress - strain curve for concrete material
(Storage period, A: 300 hrs, B: 600 hrs)

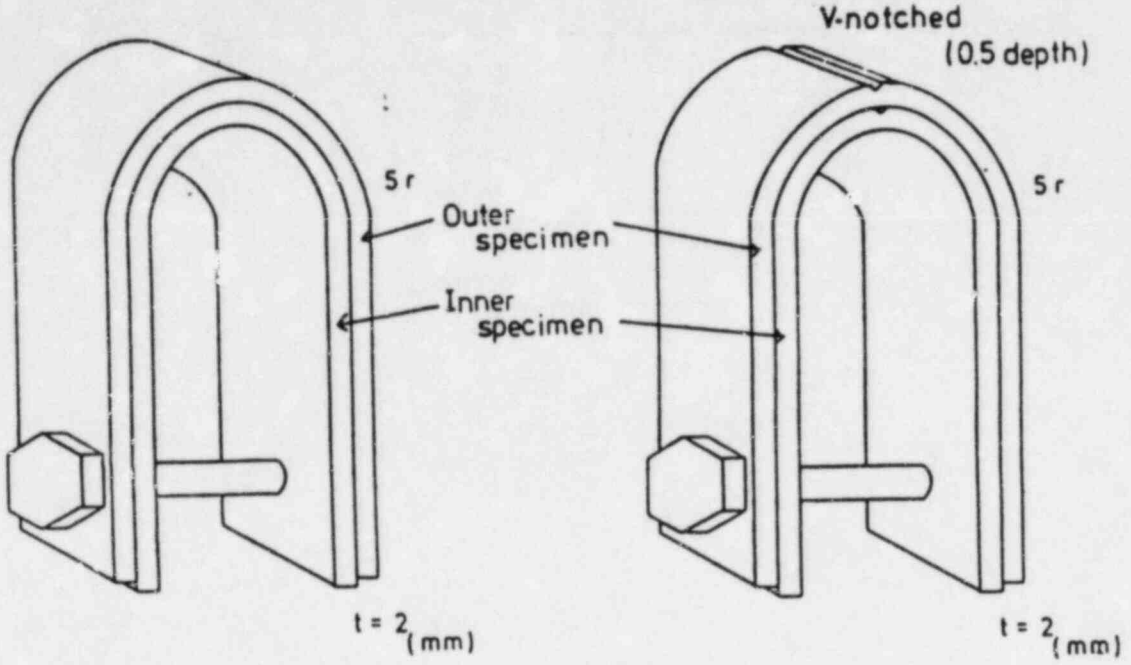

(a) Plain specimen (b) V-notched specimen

Fig. 3-3 Schematic diagram of double U-bend type specimen

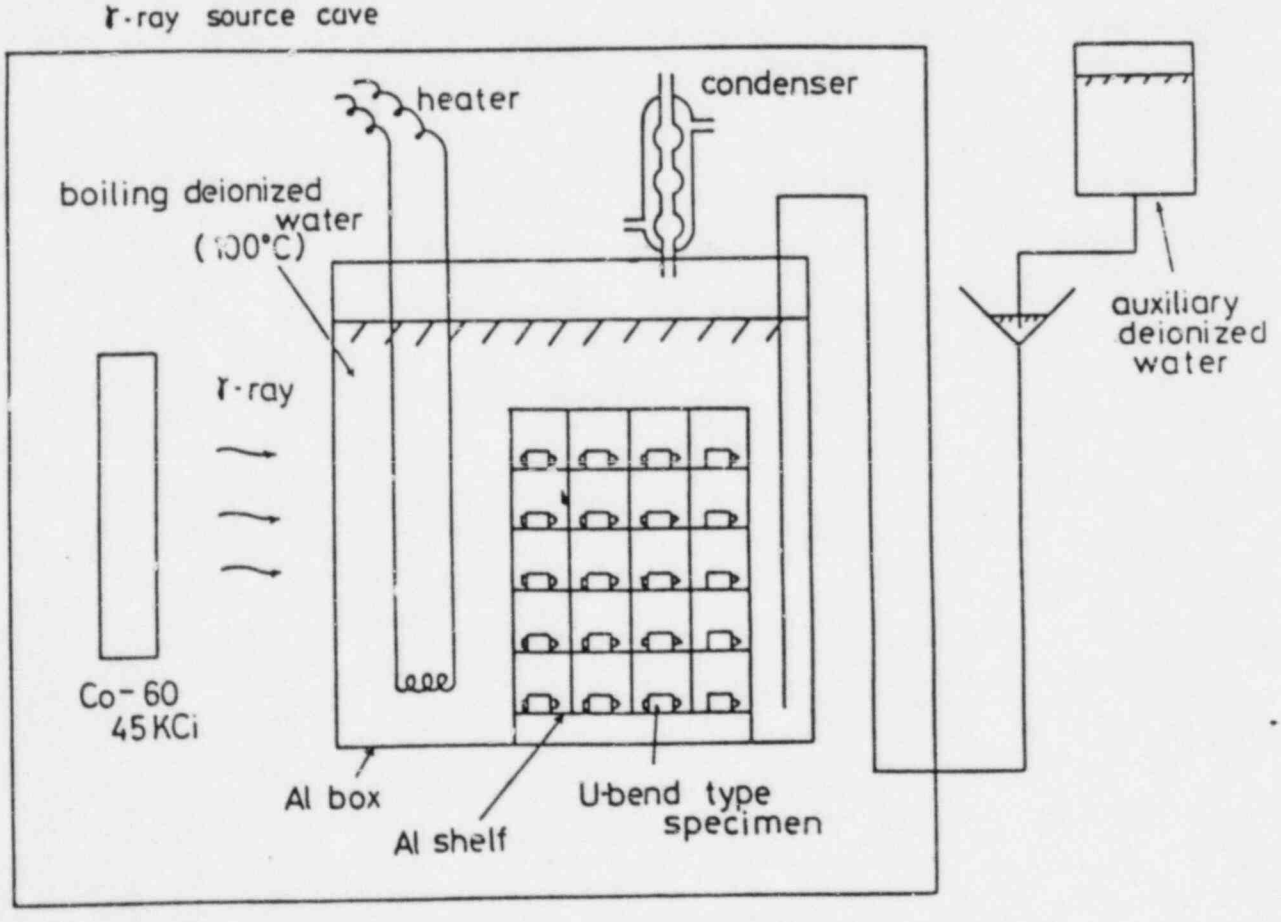

Fig. 3-4 Schematic diagram of γ-ray irradiation (First test)

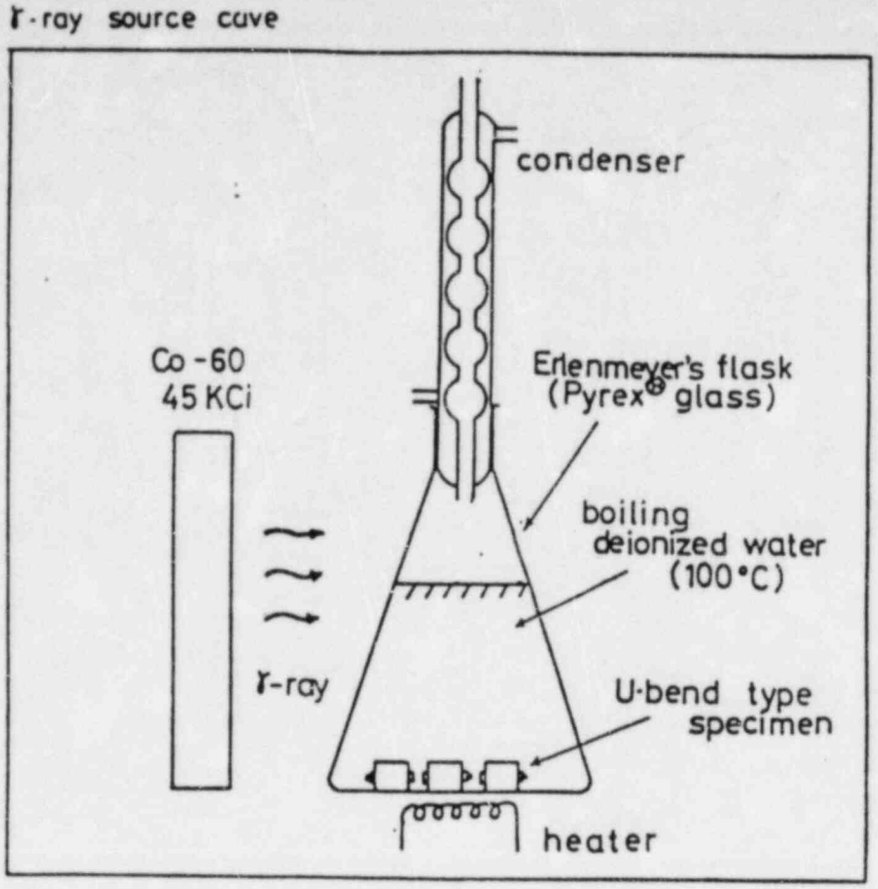

Fig. 3-5 Schematic diagram of γ-ray irradiation (Second test)

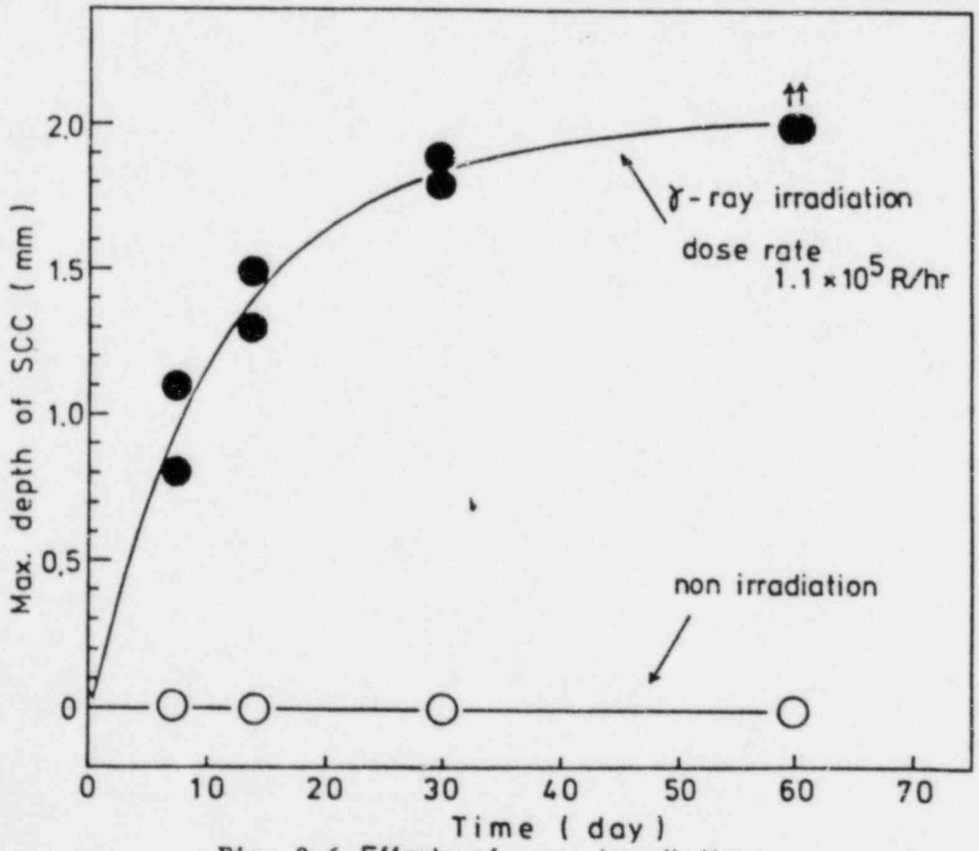

Fig. 3-6 Effects of ray irradiation on SCC failures of senstized Type 304 ss. (Second test)

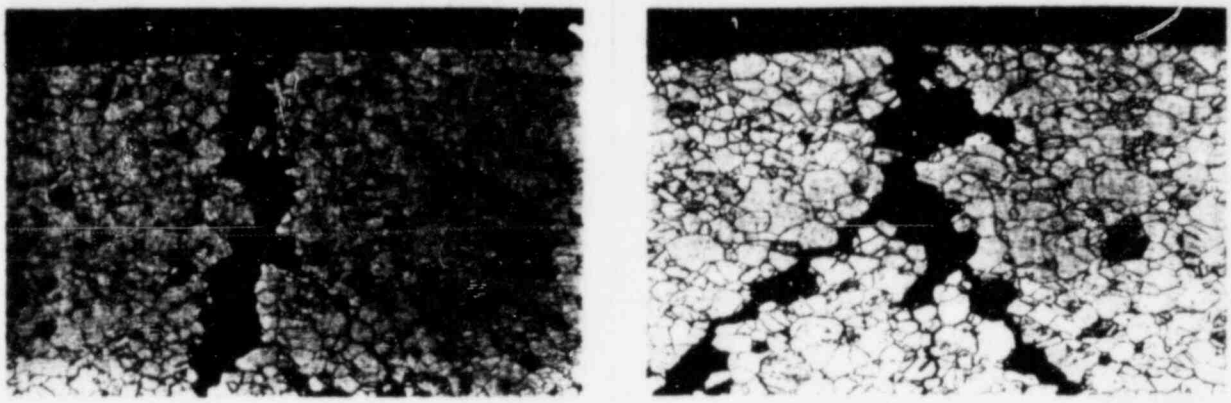

(x 100) (x 100)

Fig. 3-7 SCC modes in Type 304 SS specimen after immersion in boiling deionized water for 180 days under non irradiation (a) and γ-ray irradiation (b) (First test)

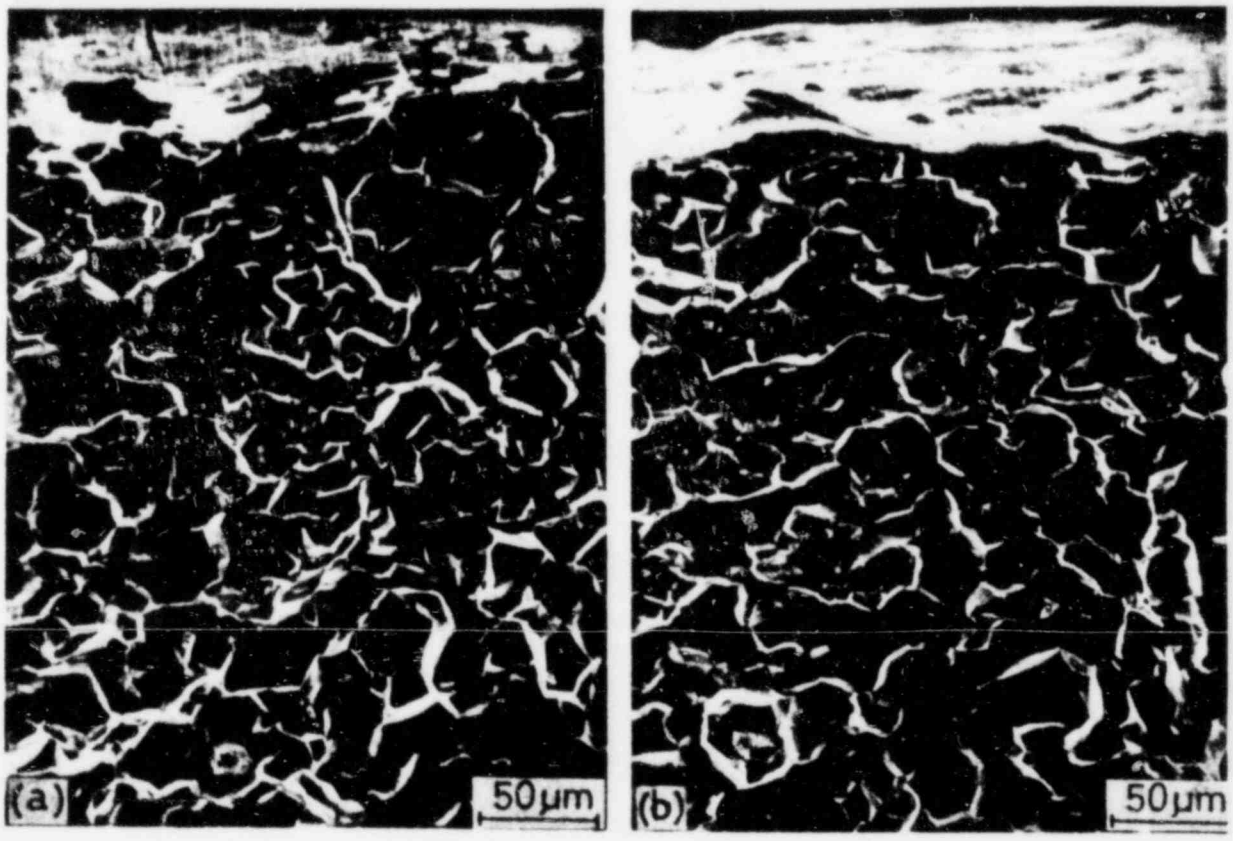

Fig. 3-8 SCC modes in Type 304 SS specimen after immersion in boiling deionized water for 180 days under non irradiation (a) and γ-ray irradiation (b) (First test)

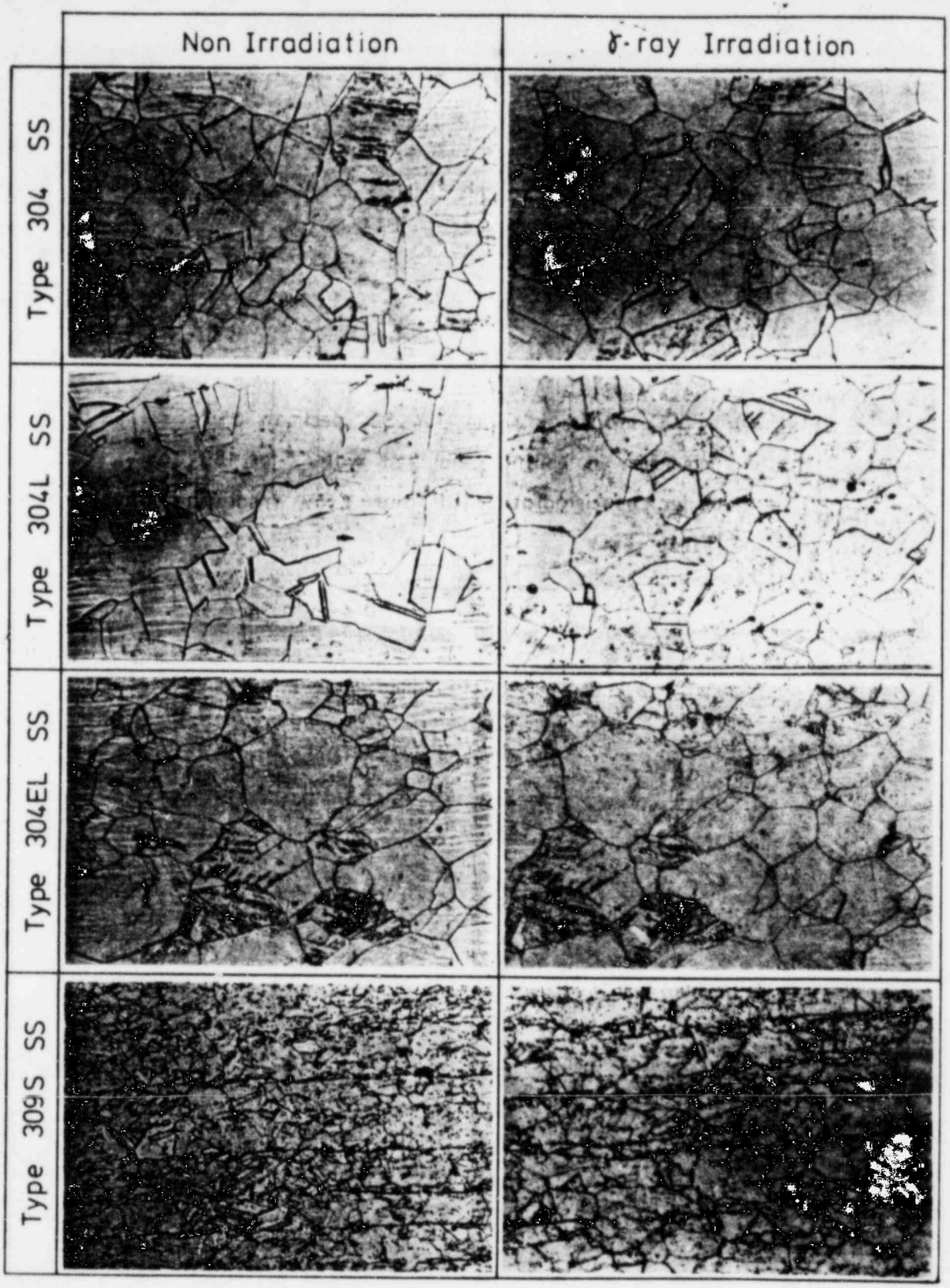

Fig. 3-9 Comparison between γ-ray irradiation and non irradiation on the microstructure of alloys after immersion for 180 days in boiling deionized water (First test)

4. Safety evaluation of geologic disposal

4.1 Nuclide migration code

H. Kimura

On the estimation of radionuclide migration in the geologic media by mathematical model, two different approaches have been developed by many researchers. One is termed the "model-equation" method[1] which is based on transport equations of radionuclide in the geologic media. Usually these equations are solved by using finite-difference or finite-element techniques with the appropriate initial and boundary conditions. Another approach is the "direct-simulation" method which defines numerical structures represent specific constituents or physical structures of migration process. The direct-simulation method requires that an efficient bookkeeping structure is established to control the response of the numerical representations so that all physical constrains are satisfied. This method has following advantages;

(i) It is always mass conservative.
(ii) There is no cumulative numerical dispersion.
(iii) There is inherent numerical stability.
(iv) It facilitates handling of multicomponent systems.

The direct-simulation technique for transport analogue was developed by Eliason and Foote[2] and Ahlstrom et al.[3]. Washburn et al.[4] developed Multicomponent Mass Transport (MMT1D) code to predict one-dimensional migration at Pacific Northwest Laboratories using direct-simulation method. We have adopted the same treatment as the above stated models about transport description. In MMT1D, decay chain is dealt with such a model that new daughter particles are created around their parent particles at random every time step. We have introduced decay probability and dealt with decay chain as particle's character change.

Mathematical model

(1) Transport description

The material dissolved or suspended in the ground water is represented as an ensemble of a finite number of discrete particles. All particles move with the continuum of ground water and at its velocity. Each particle has a defined location and a finite radioactivity associated with it. The particles are independent and occupy zero volume. The driving forces for particle movement are convection and dispersion in the ground water. The retardation of nuclide migration is accounted for by dividing the velocity and dispersion coefficient by retardation coefficient. Total movement of particle is given by eq.(1). (Eq.(1) is one-dimensional expression to understand easily.)

$$X = X_0 + \Delta t \cdot \frac{V(X_0)}{Rd(X_0)} + \sqrt{\frac{24 \cdot D \cdot \Delta t}{Rd(X_0)}} \cdot (0.5 - [R]_0^1) \qquad (1)$$

where

X	;	new location of particle after Δt
X_0	;	old location of particle
Δt	;	time step
$V(X_0)$	;	water velocity at X_0
$Rd(X_0)$	;	retardation coefficient of nuclide at X_0
D	;	dispersion coefficient
$[R]_0^1$	;	random number between 0 and 1 from a uniform distribution

(2) Concentration of nuclide

In order to calculate the concentration, particle distributed space is divided into unit cell. The concentration of nuclide C_A is given as follows.

$$C_A = \frac{G_A \cdot N_A\ (i,j,k)}{\Phi(i,j,k)} \qquad (2)$$

where

G_A ; activity of one particle A

N_A (i,j,k) ; number of particles A in the cell (i,j,k)

Φ (i,j,k) ; water volume of the cell (i,j,k)

(3) Decay chain treatment

In this model, radioactive decay is taken into account every time step about each particle. If parent particle decays during time step Δt, parent particle changes to daughter particle. Characters of particle change at its time step. Probability of decay from nuclide A to nuclide B $P_{A \to B}$ is given by eq. (3).

$$P_{A \to B} = 1 - \exp(-\lambda_A \cdot \Delta t) \qquad (3)$$

where

λ_A ; decay constant of nuclide A

If produced random number $[R]_0^1$ is less than $P_{A \to B}$, radioactive decay occurs. Then due to character change, behavior of particle changes from A to B. (Flow chart of calculation is shown in Fig. 4-1)

Calculated result

Our model was compared with analytical model MGRATO3[5]. As MGRATO3 is one-dimensional model, nuclide migration in one-dimensional case are calculated in our model. Compared result is shown in Fig. 4-2 for three-member decay chain comprised of ^{237}Np, ^{233}U and ^{229}Th. Table 4-1 summarized the input data.

References

1) Dillon, R.T., et al. "Risk Methodology for Geologic Disposal of Radioactive Waste: The Sandia Waste Isolation Flow and Transport (SWIFT) Model "NUREG/CR-0424 (1978)

2) Eliason, J.R., and H.P. Foote, "Long Beach Generation Station Thermal Transport Modeling Study" Prepared for the Southern California Edison Company 2120133F (1972)

3) Ahlstrom, S.W., et al. "Multicomponent Mass Transport Model: Theory and Numerical Implementation: BNWL-2127 (1977)

4) Washburn, J.F., et al. "Multicomponent Mass Transport Model: A Model for Simulating Migration of Radionuclides in Ground Water" PNL-3179 (1980)

5) Harada, H., et al. "Migration of Radionuclides through Sorbing Media Analytical Solutions-I" LBL-10500 UC-11 (1980)

6) Yamagata, S., et al. "Study on distribution coefficient for cesium between granite and water (Note)" JAERI-M 9432 (1981)

4.2 Field tests

4.2.1 In-situ measurement of heat transfer and thermal stress in schalstein rock mass

K. Shimooka

One of the most important impacts to the stability of a repository for the high level waste is the thermal disturbance from the decay heat, which has been investigated by in-situ experiments in many countries.

Field tests to investigate the heat transfer in-situ have been conducted since the end of 1977 by JAERI.

It was found that the value of the thermal conductivity of a rock mass in-situ was bigger than those of core samples in a laboratory, the water in a rock mass was liable to increase the thermal conductivity.

The behavior of water was investigated.

Temperature distribution and thermal stress were measured to clarify the mechanism of influence of water on heat transfer.

Experimental

The drift at the depth of 380 m under the earth surface in Akenobe Mine was used for the heater experiments.

The rock mass consists of a schalstein of Permian age.

Mineral components are chlorite, plagioclase, quartz, epidote and pyroxene.

Columnar section of boring core was shown in Fig. 4-3.

Two 48 mmϕ holes for measuring water content (No.10) and thermal stress (No. 9) and eight 29 mmϕ holes for electric heaters (No. 1, No. 2) and thermocouples (No. 3 ∿ No. 8) were drilled as shown in Fig. 4-4.

Electric heaters were designed and made with nichrom wire surrounded by magnesia insulation and sheathed in 2.2 m length and outer diameter of 25.4 mm SUS 304 pipes.

The electric power of the heaters were kept constant at around 2 kW for 47 days and after 26 days cooling time the power was raised to 4kW and ketp for 48 days.

Temperatures were measured by the twenty Chromel-Alumel thermocouples which were placed in each boreholes as shown in Fig. 4-4.

The accuracy of temperature measurement was 0.1°C.

Water content of the rock mass was measured by neutron scatter method with using ^{252}Cf (∿90μCi).

The thermal deformation of the rock mass was measured by strain meters made by Kyowa Dengyo Co..

Results

The relation between observed temperature and calculated one at 2 kW heating was shown in Fig. 4-5.

Temperatures at the positions of thermocouple No. 63, 73 and 83 did not reach the calculated temperature but was hold constant around 100°C.

The temperature increase at 4 kW heating was shown in Fig. 4-6.

Temperature at the point of 73 rose sharply after 25 days.

This constant temperature and the sharp increase are liable to be explained by vaporization of water in the rock mass.

The water content of a rock was about 1.4 weight %.

Temperatures at the point of 41, 42, 71 and 75 were raised higher than the calculated temperatures.

Higher temperature at this area may be due to the result of the heating by condensation and/or the heating by the moved hot water.

In No. 5 and No. 9 boreholes where the leakage of water was seen, lower temperatures were observed.

At the position of thermocouple number 33, the far point from the heaters where estimated maximum temperature does not exceed 100°C and also seemed to be dry area, the calculated temperature by using the core sample's thermal conductivity; 2.9 W/m/°C, agreed with the observed one very well.

It was found that the temperature distribution in a

sphere, dry and with a low temperature of under 100°C could be estimated by using heat conduction.

But in the high temperature sphere which included water, transportation of the heat was complicated because of the behavior of water.

The thermal strain at the surface of the drift near heater horeholes began to be induced after heating time of 2 days.

The tensile strain of 4500×10^{-6} and 3000×10^{-6} were observed after heating of 46 days.

The change of the strain in the rock mass with temperature was shown in Fig. 4-7.

The increase of the compressive strain in the direction of X and Y was almost the same.

But the strain in the direction of Z was bigger than those of X and Y directions. The work was performed by Mitsubishi Metal Corporation Ltd. under a contract with JAERI.

4.2.2 Migration of ions in fractures S. Muraoka

Migration of nuclides was studied in a real environment in situ for safety assessment of the HLW geological disposal. Retardation of the migration is due to the sorption of ions on minerals, not only in a rock but also in a fracture. The latter one is usually clay minerals, so it must be more predominant because of its larger ion exchange capacity. Importance of in situ test is that natural and real structure of the fracture is only available in situ.

Experimental

The situ of the experiments is the same one used for heat conductivity test described above. No. 9 hole was used for charging solutions containing ions. Double packers were inserted to hole at about 18 cm and 68 cm depth as shown in Fig. 4-8. The solution was charged in at 4 kg/cm^2 pressure by compresser. Water appeared at position A-D on the wall of the drift, which was collected with funnels fixed on the wall as shown in Fig. 4-9. No leakage of the solution to the other testing holes was observed.

LiI, $CsNO_3$, $Ba(NO_3)_2$, $Sr(NO_3)_2$ and $ZrO(NO_3)_2$ were disolved by water to prepare the solutions of 50 - 100 μg/ml of metal elements. Concentrations of the ions were measured by atomic absorption method. Cs^+ ion was measured by flame emmision spectroscopy.

Result

Typical break through curves are shown in Fig. 4-10. Here C/Co is the ion concentration ratio between the effluent and initial solution. Low absorption coefficient of I^- is known by many workers. The C/Co of I^- after leveling off (0.85) shows the dilution by natural water, which agree with the values of Sr^{2+} and Cs^+. Slower effluent in position B defines the difference of retardation between Sr^{2+} and Cs^+ more clearly than in position C. The C/Co of Ba^{2+} is smaller than the one of Sr^{2+}. ZrO^{2+} was not detected or large fluctuation of the value was observed.

4.3 Laboratory tests

4.3.1 Batch Kd experiments for ^{137}Cs sorption on granite

K. Shimooka

Introduction

As a study of high-level wastes migration in geological formations, sorption of Cs on granite has been studied.

The apparent distribution coefficients (Kd) for Cs were measured under conditions with various initial concentrations of Cs from 1 μg(C_s)/mℓ to 1000 μg(C_s)/mℓ with stable cesium in the last experiments.[6)]

The results showed that the concentration effect on Kd was so large that the Kd in 1 μg(C_s)/mℓ was 100 times larger than the one in 1000 μg(C_s)/mℓ.

But a value was expected to level off in lower concentration than 1 μg(C_s)/mℓ.

The experiments with $^{137}C_s$ were carried out to measure the Kd in the range of $1 \times 10^{-5} \sim 10$ μg(C_s)/mℓ of initial concentrations.

Experimental

Granite used in the experiments was sampled from Inada, Ibaraki prefecture.

Each 20g of granite was powdered and added into each 200 mℓ of cesium solutions in the range of 10^{-5}, 10^{-4}, 10^{-3}, 10^{-2}, 10^{-1}, 1 and 10 μg(C_s)/mℓ including 0.648 μCi of ^{137}Cs as a tracer.

The ratio of solution volume to weight of granite was 100 mℓ/g.

Contact period was 98 days, while the samples were left at room temperature and ocasionally agitated.

The supernatant solutions were withdrawn and the beta activities were counted with a proportional counter on evaporated and dried samples.

The pH values of the solutions were measured with pH testing papers.

Result

Apparent Kd were represented by the ratio of activity concentration in solid and in solution.

Even at in the low concentration around 10^{-2} μg(C_s)/mℓ, the effect of C_s concentration on Kd was observed.

But no effect was found at the range under 10^{-3} μg(C_s)/mℓ.

The Kd values increased with decreasing cesium concentration from about 50 mℓ/g at 10^{-1} μg(C_s)/mℓ to about 170 mℓ/g at 10^{-6} μg(C_s)/mℓ.

The influence of contact time on sorption was shown in Fig. 4-12.

A trend of increasing Kd with increasing contact time was observed for all initial concentration samples of 10^{-5}, 10^{-4}, 10^{-3}, 10^{-2}, 10^{-1} and 1 μg(C_s)/mℓ.

The increase in Kd with increasing contact time suggested that the equilibrium was not established even after contact time of 98 days.

This behavior is caused by the diffusion of cesium into the rock minerals and by the chemical change at the surface of rock samples and by an effect of pH change of the solution.

The dependence of Kd value on cesium concentration will require the more complicated transport models and also the validation experiments in the geological formations.

So, in-situ measurements of the sorption behavior in a rock mass have been carring out now.

4.3.2 Hydrothermal interactions between simulated high-level waste glass and natural rocks

M. Kumata

Introduction

The main threats to the effective isolation of radionuclide from biosphere is the disolution of the waste and subsequent radionuclide transport by graundwater from repository in deep geological formations.[1] Accordingly, one of the important consideration is the stability of the waste forms and surrounding rocks in the repository environment. In a sealed nuclear waste repository hydrothermal conditions may arise because of the heat generated by radioactive decay.[1),2)]

From this point of veiw, hydrothermal interactions of granite and basalt as repository rocks with simulated high-level waste (HLW) glass have been examined.

Experimental

1) Materials

The two natural rocks used in this study were biotite granite and olivine basalt. The biotite granite is composed of quartz, feldspar, biotite and a small amount of magnetite. On the other hand, the olivine basalt is composed of feldspar, olivine, a small amount of augite and a significant amount of glass as the primary phases.

The simulated HLW glass used in these experiments was a borosilicate glass containing 20 wt% of simulated high-level waste.

The rocks and glass were crushed and dry ground to under 200 mesh (< 75 μm). The powdered rocks and glass were mixed with ratios of rock/glass as 1:1. Then, they were cold-pressed (580 kg/cm^2) and used in the experiments.

2) Methods

A weighed cold-pressed specimen was contained in the gold capsule with ion exchanged water. Fluid/solid ratio was 10 to 1.

The experiments were performed in gold plated pressure vessel using water as the pressurizing medium. The temperature was nominally 300°C, and the pressure was 300 bars. Run duration was 30 days.

The residual solid and liquid phases from all run capsules were saved for analyses. The solid samples were dried for X-ray diffraction analysis, an optical microscope, scanning electron microscope (SEM) and electron probe micro analysis (EPMA). The solutions were analyzed by Atomic Absorption Spectrophotometry (AAS) and Inductively Coupled Plasma (ICP) method.

Results and Discussion

From analyses of the liquid phases from hydrothermally treated mixtures of granite or basalt with simulated HLW glass, following elements were ditected by AAS or ICP method; silicon, sodium, iron, calcium, aluminium, magnesium, potassium and cesium but not ditected strontium which was included in simulated HLW glass at about 0.3 wt% as simulated radwaste element.

Analyses of the solid phases by optical microscope, SEM and EPMA revealed that a few new crystalline phases were formed during hydrothermal treatment. One of them is mainly composed of silicon, sodium and cesium.

References

1) G. J. McCarthy, W. B. White, R. Roy, B. E. Scheetz, S. Komarneni, D. K. Smith and D. M. Roy ; Nature, 273, 216 (1978).

2) S. Komarneni and B. E. Scheetz ; J. Inorg. Nucl. Chem., 43, pp. 1967-1975 (1981).

4.4 Stress around the repository

S. Muraoka

Stress and heat will be generated in a repository for radioactive wastes by exacavation and decay heat from the HLW. Stress and thermal effects on rock formation surrounding the repository have been estimated and analysed as a point of important consideration in the case that the repository is designed and constructed in deep underground. By these studies, subjects to be studied are presented in relation to safety geologic disposal. Data about properties of rocks at room and high temperatures (100-500°C) were surveyed. However high temperature data were not available at the moment except a few kinds of rocks. It would be necessary to compile such data and to clarify the influence of water content and fractures in rock formation by not only in laboratory examination but also tests in the rok formation in situ.

Temperature distribution in near field of the repository was calculated by NASTRAN, code for structural and thermo-mechanical analysis. As a example of the results, Fig. 4-13 shows a vertical profile of the temperature distribution along the centerline of the repository tunnel. In the figure Case 1 corresponds to the temperature distribution after back-filling the tunnel and Case 2 corresponds to the one before the back-filling. Comparison of these two cases indicates the effect of cooling by ventilation through the tunnel on the temperature distribution.

Central temperature of buried waste package is calculated to be 470°C with the consevative assumption of the boundary condition. This suggests a necessity of examination of rock formation around 400°C.

Stress around the repository tunnel was also calculated. As shown in Fig. 4-14 it is found that the region of strength failure is held in the condition just after excavation, but the region spreads in the case of no ventilation after back-filling the tunnel.

On rock burst problem with many difficult phenomena, it is suggested to adopt a design to generate no stress concentration on the surface of the repository tunnel.

This work was carried out in cooperation by JAERI and Mitsui Construction Company Ltd.

Reference

1) National Aeronautics and Space Administration, "NASTRAN theoritical manual", NASA, 1972

Table 4-1 Input data used for comparison

Nuclide data

nuclide	inventory (Ci)	decay const. (1/yr)	retardation coefficient
Np-237	10.0	3.2 E-7	2400
U-233	10.0	4.3 E-6	2000
Th-229	10.0	9.4 E-5	5000

Hydrologic data

velocity of ground water flow	100 m/yr
dispersion coefficient	1000 m^2/yr
leaching time	4000 yr

Table 4-2 Variation of K_d with cesium concentration

Final C_s concentration [g/ml]	PH		K_d [ml/g]
	initial	final	
2.5	2	6	30
1.6×10^{-1}	2	6	53
5.5×10^{-3}	2	6	170
8.8×10^{-4}	2	6	103
5.2×10^{-5}	2	6	182
6.1×10^{-6}	2	6	155
5.9×10^{-7}	2	6	159

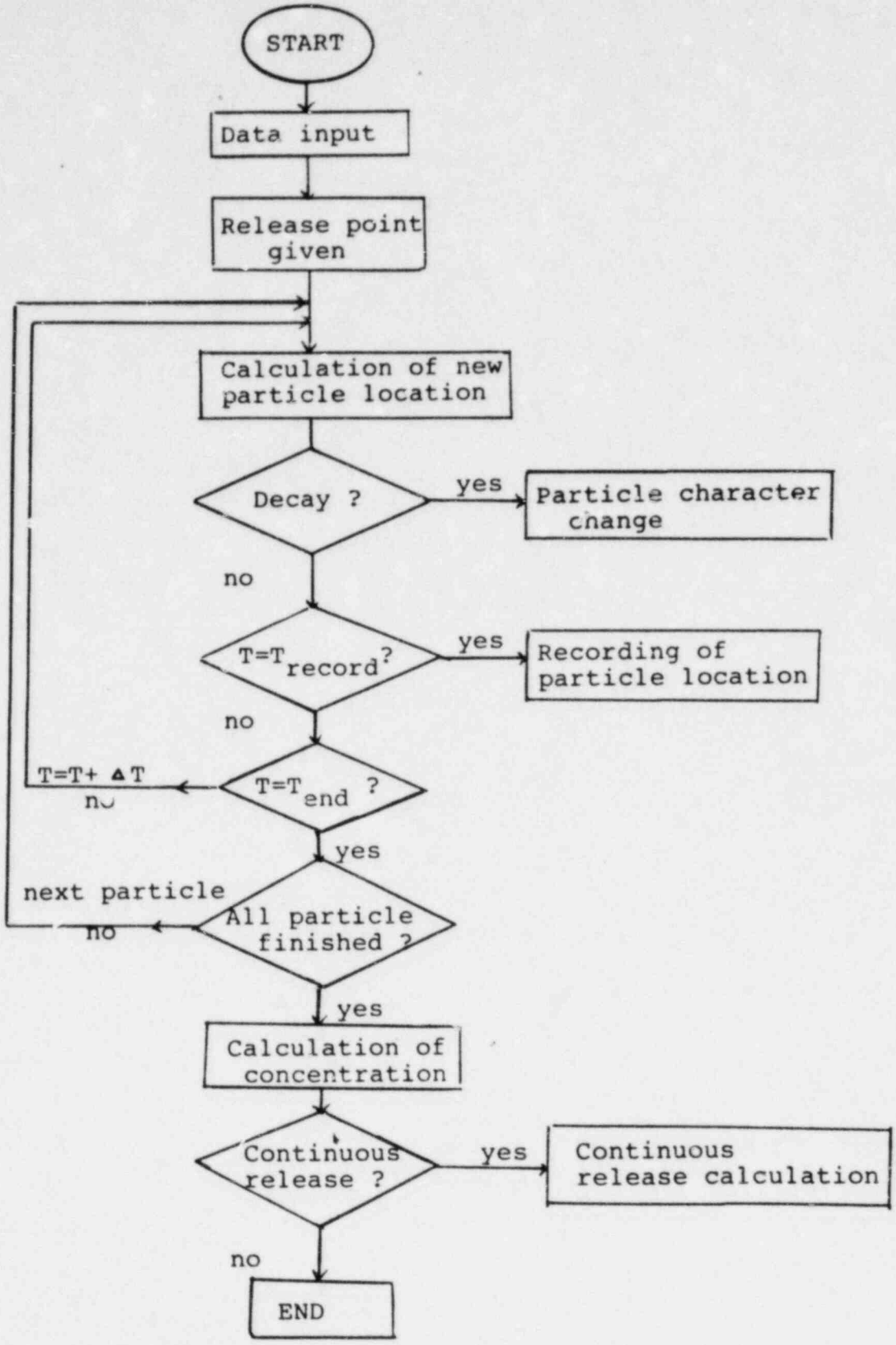

Fig. 4-1 Flow chart of calculation

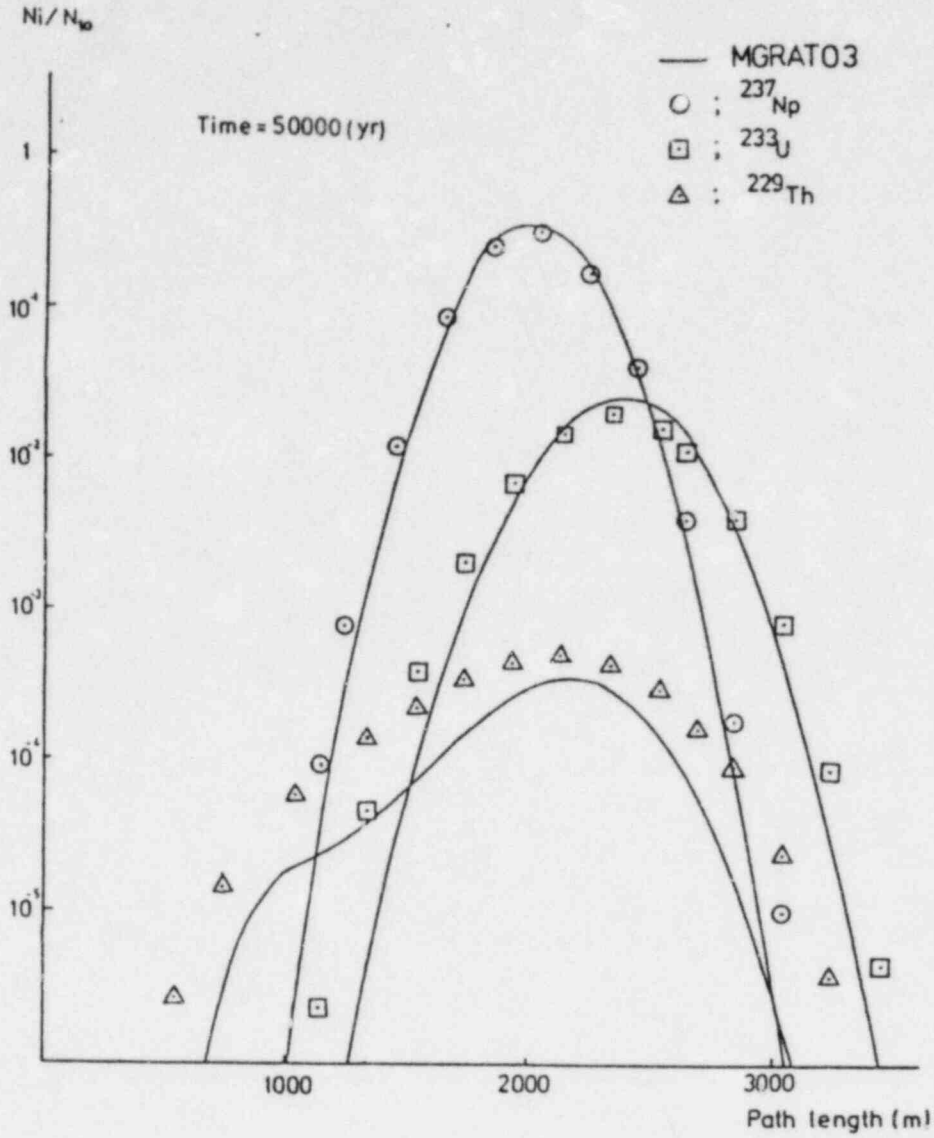

Fig. 4-2 Comparison with MGRAT03

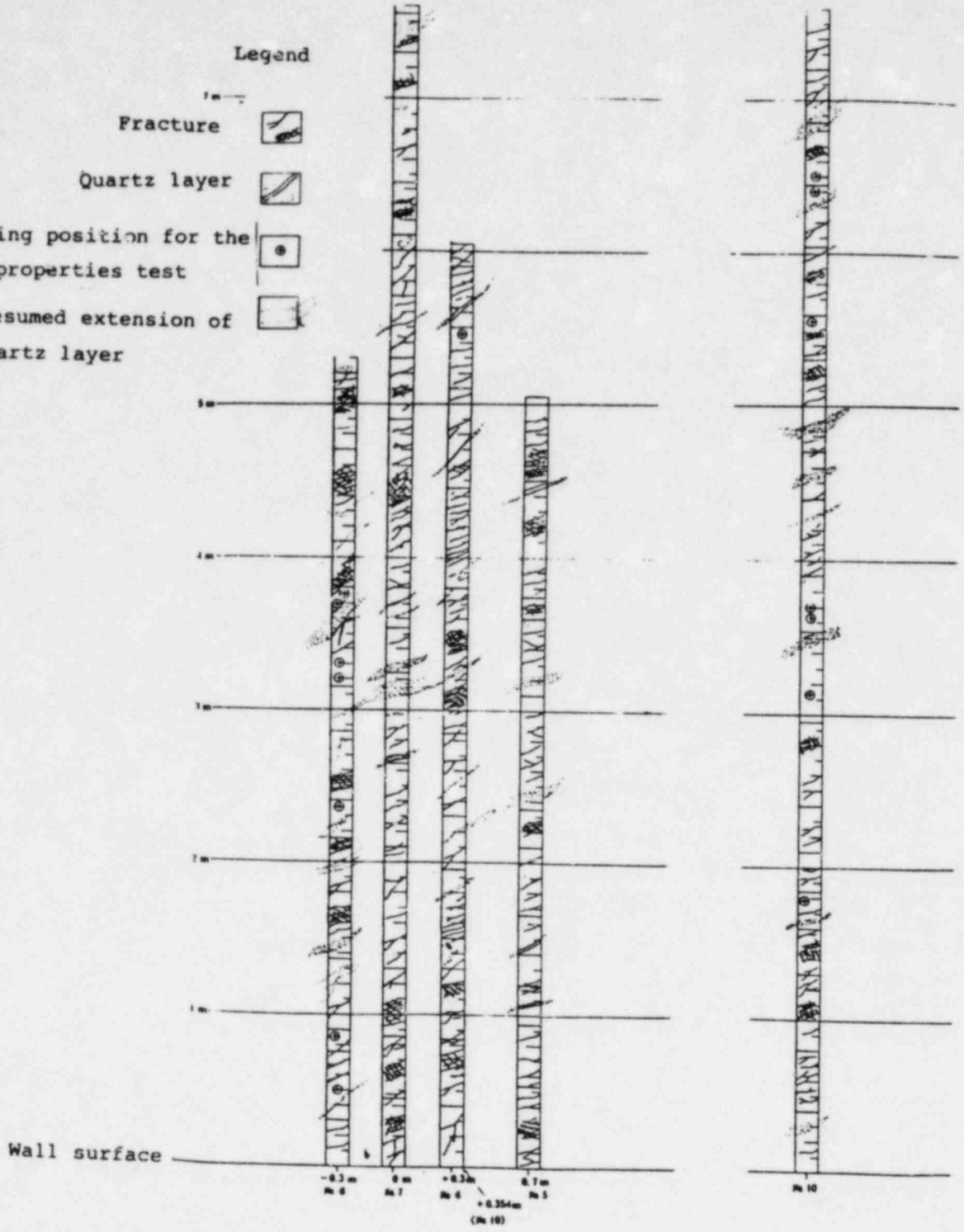

Fig.4-3 Columnar section of boring core

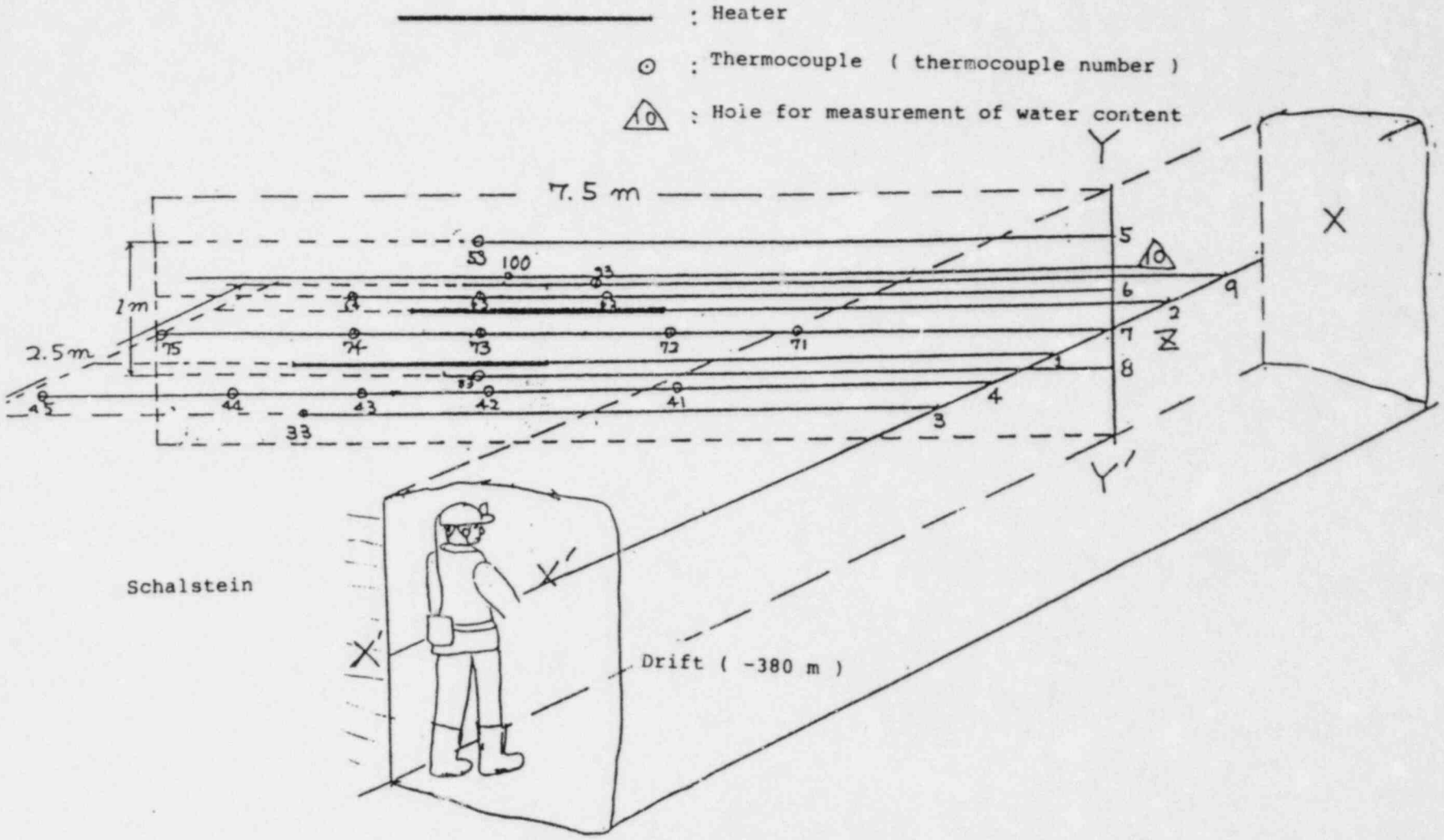

Fig. 4-4 Layout of heaters and thermocouples

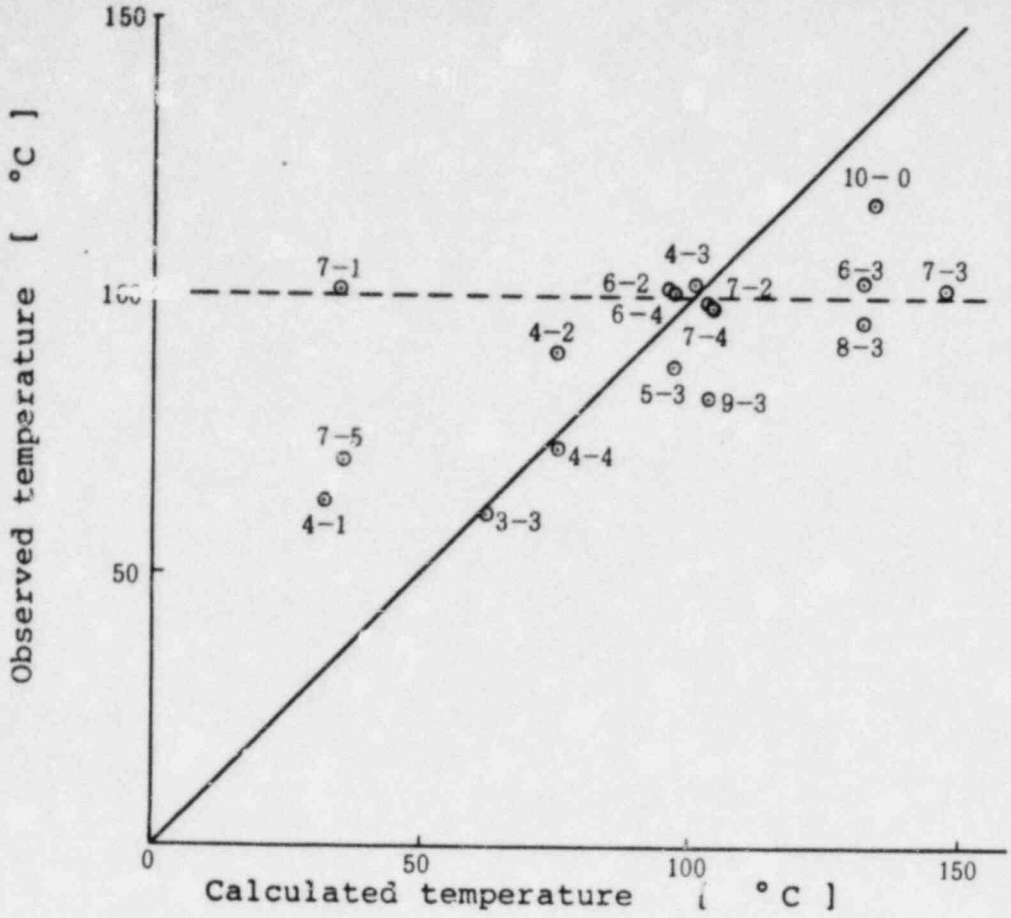

Fig.4-5 Comparison of the temperatures observed and calculated after 45 days

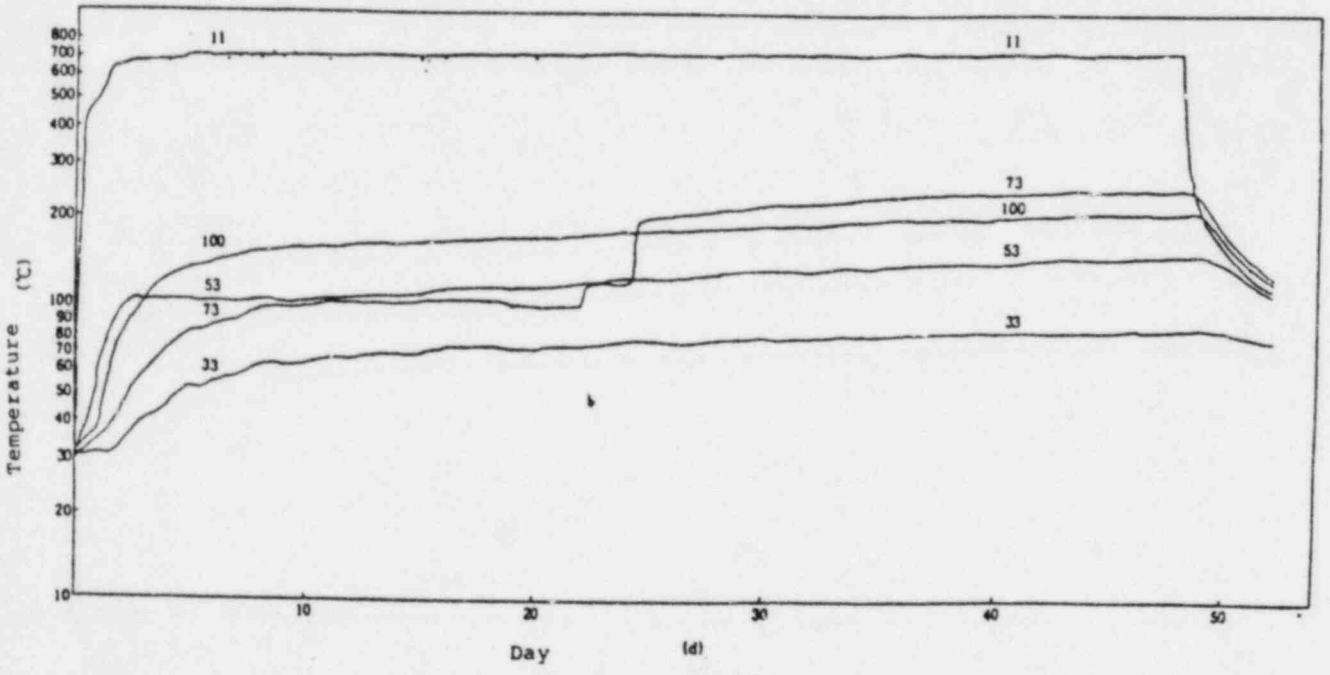

Fig. 4-6 Temperature change at 4 KW heating

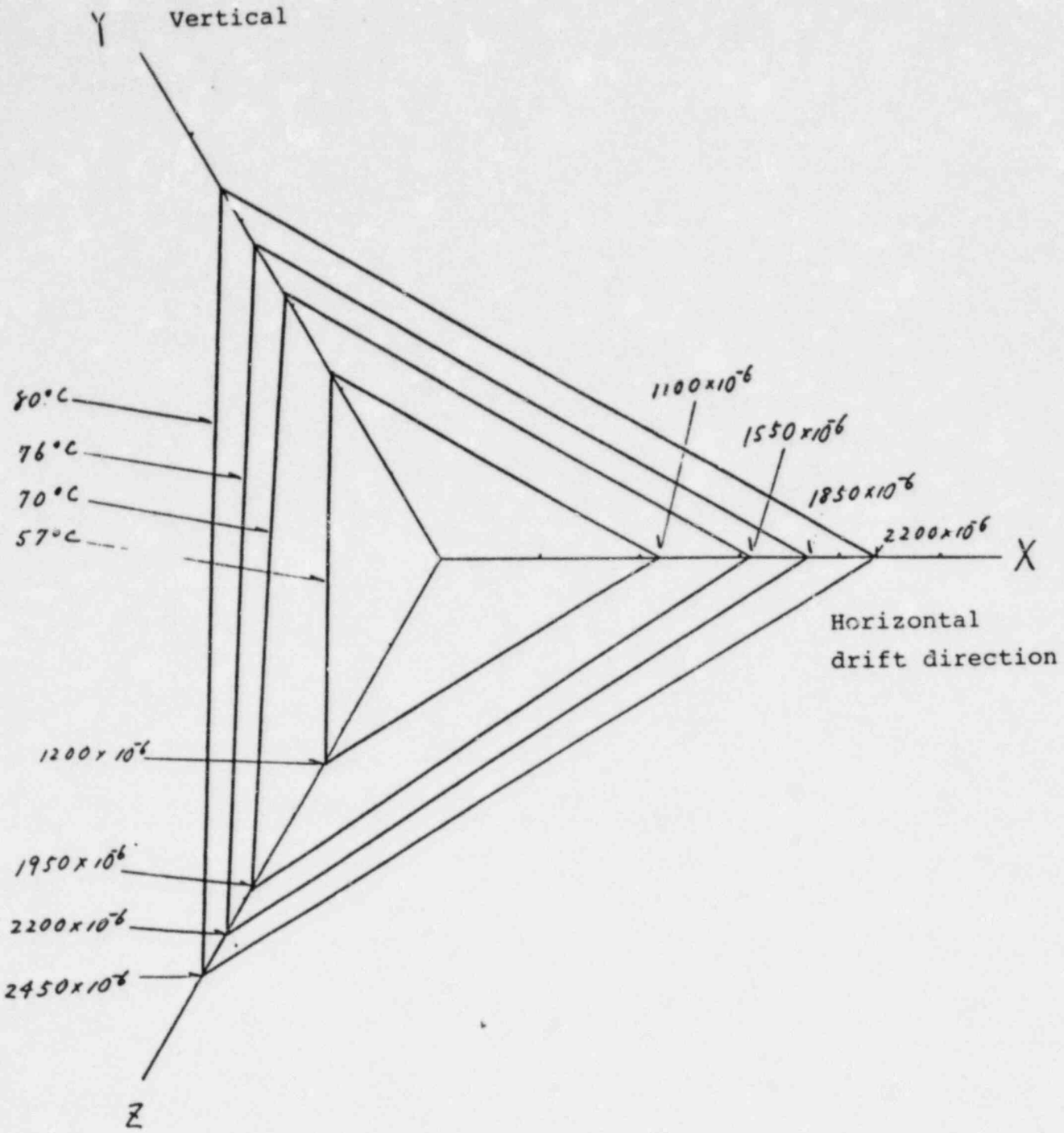

Fig. 4-7 The thermally induced strain in the rock mass

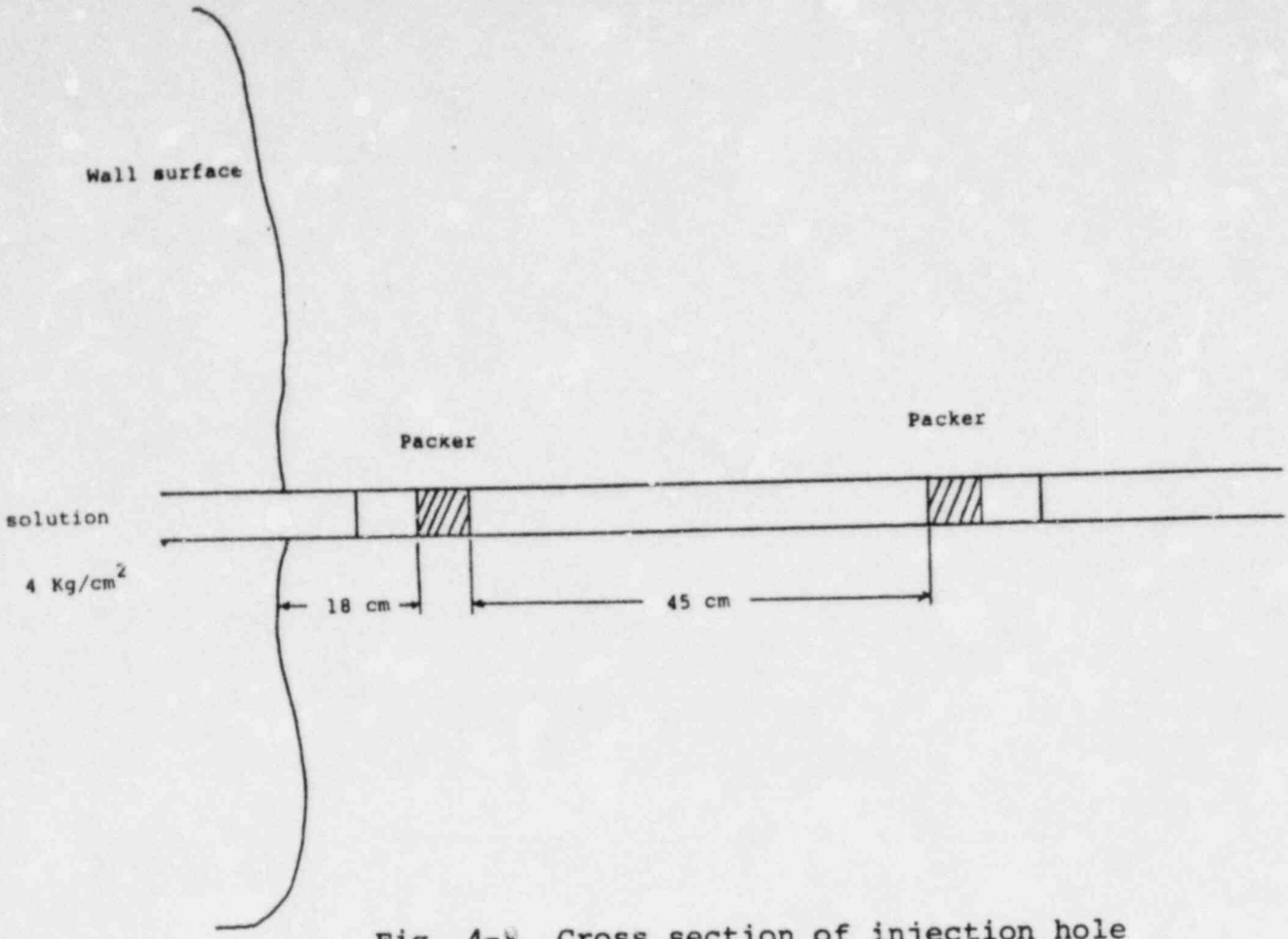

Fig. 4-8 Cross section of injection hole

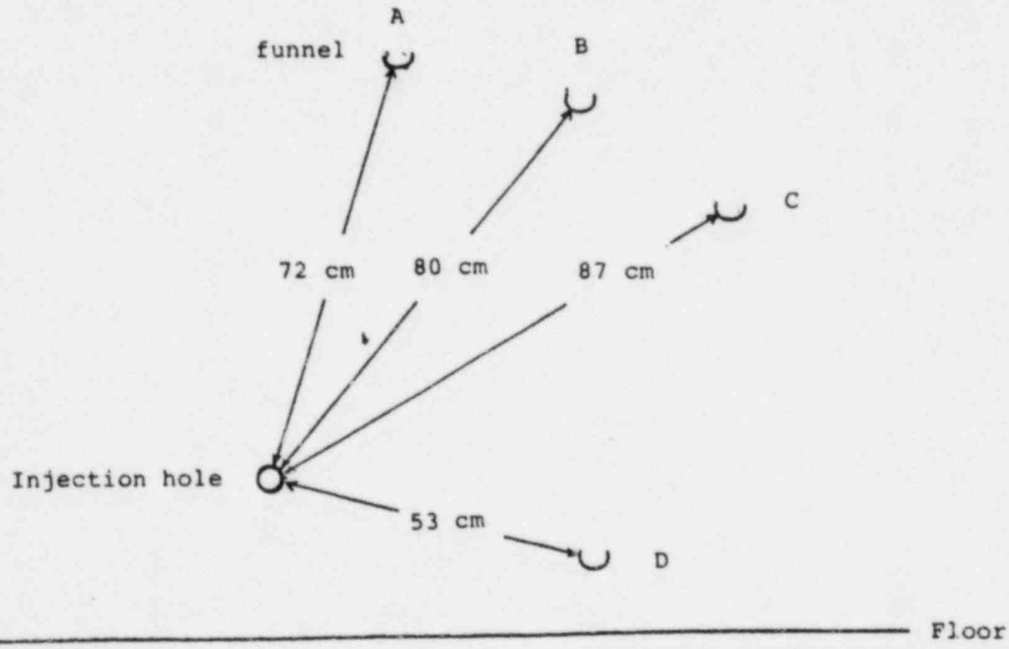

Fig.4-9 Layout of sampling position and injection hole

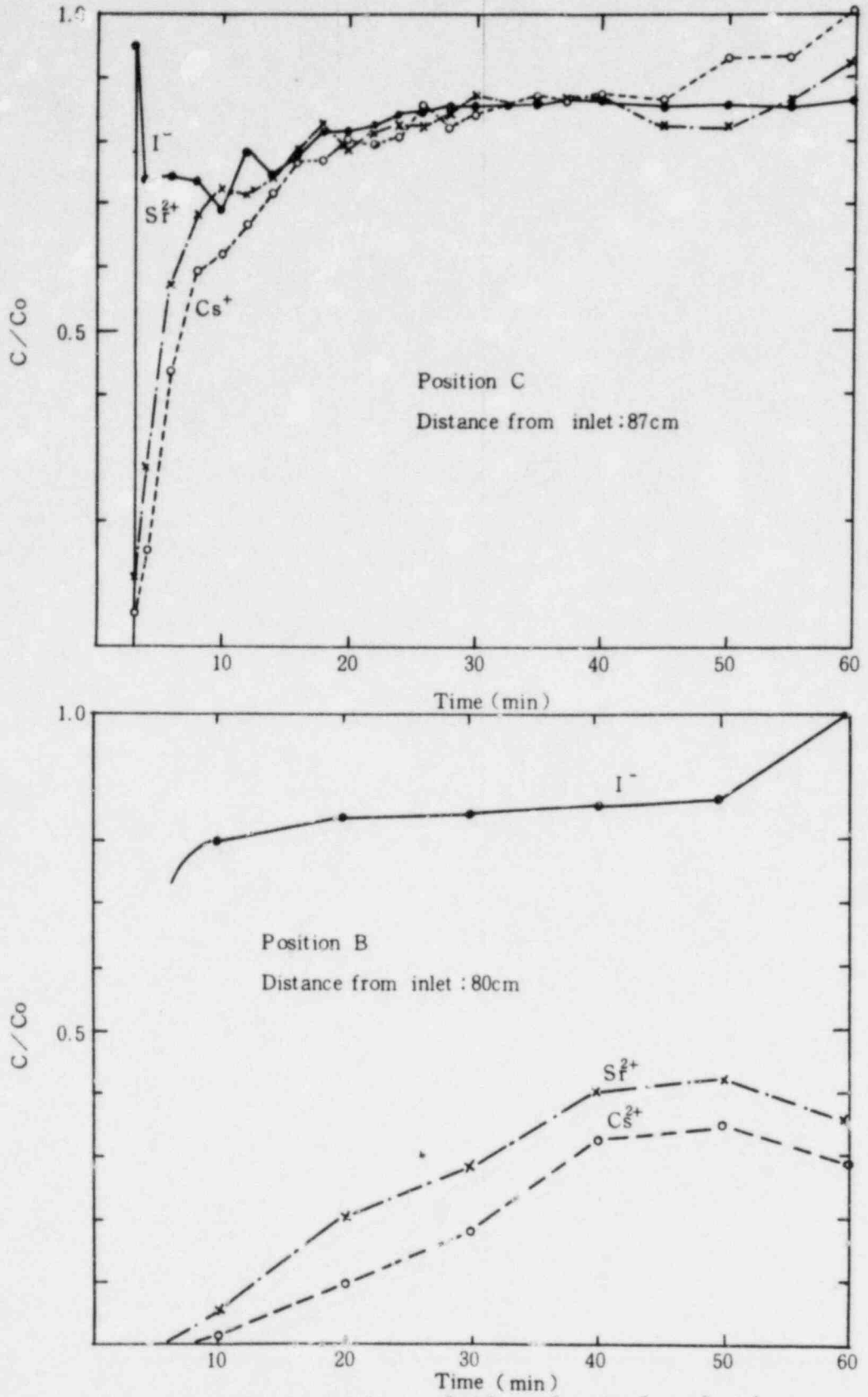

C_0: Concentration of the charged solution

C : Concentration of effluent

Fig. 4-10 Break through curves of ion from fissures in rock mass

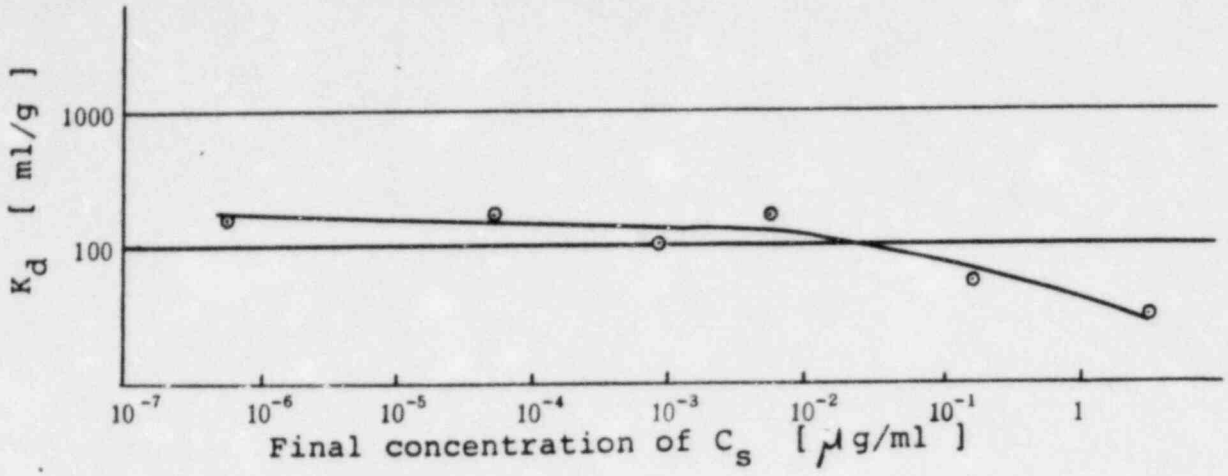

Fig. 4-11 K_d at various final concentration of cesium

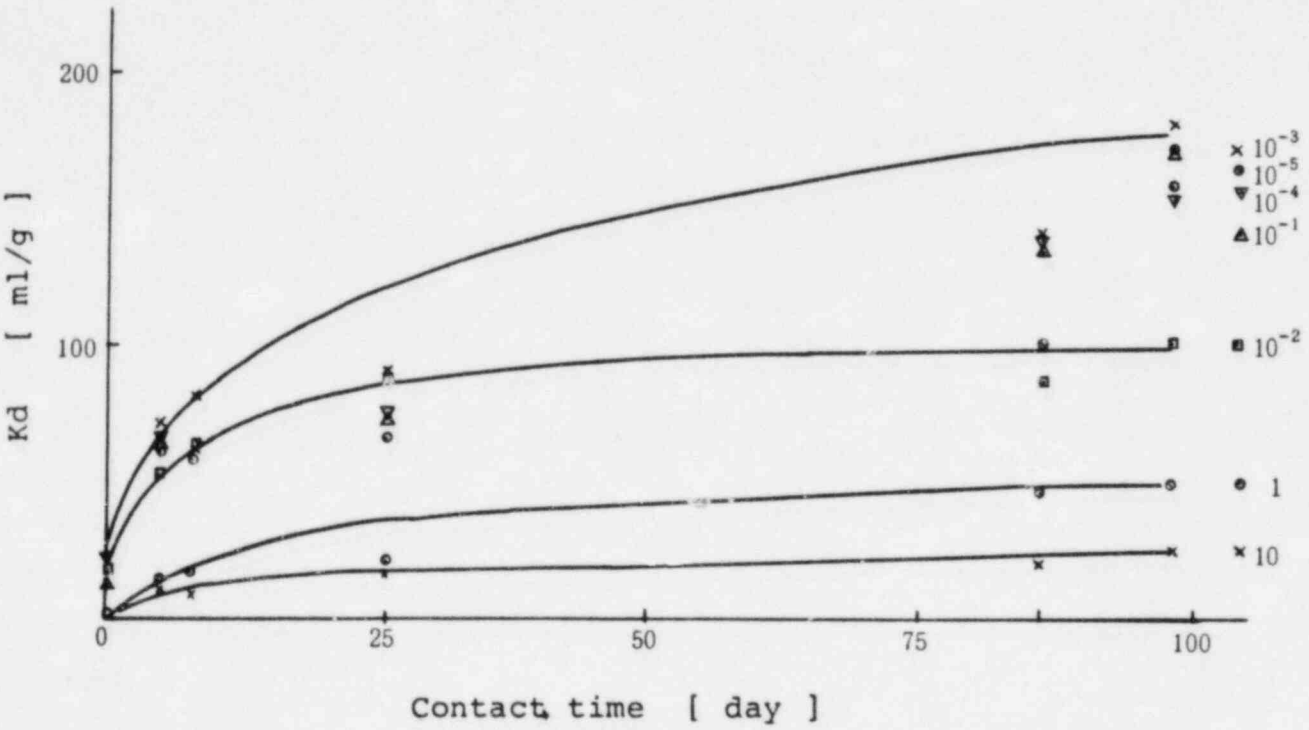

Fig. 4-12 Influence of contact time on sorption of C_s on granite with initial concentration from 10^{-5} to 1 μg/ml

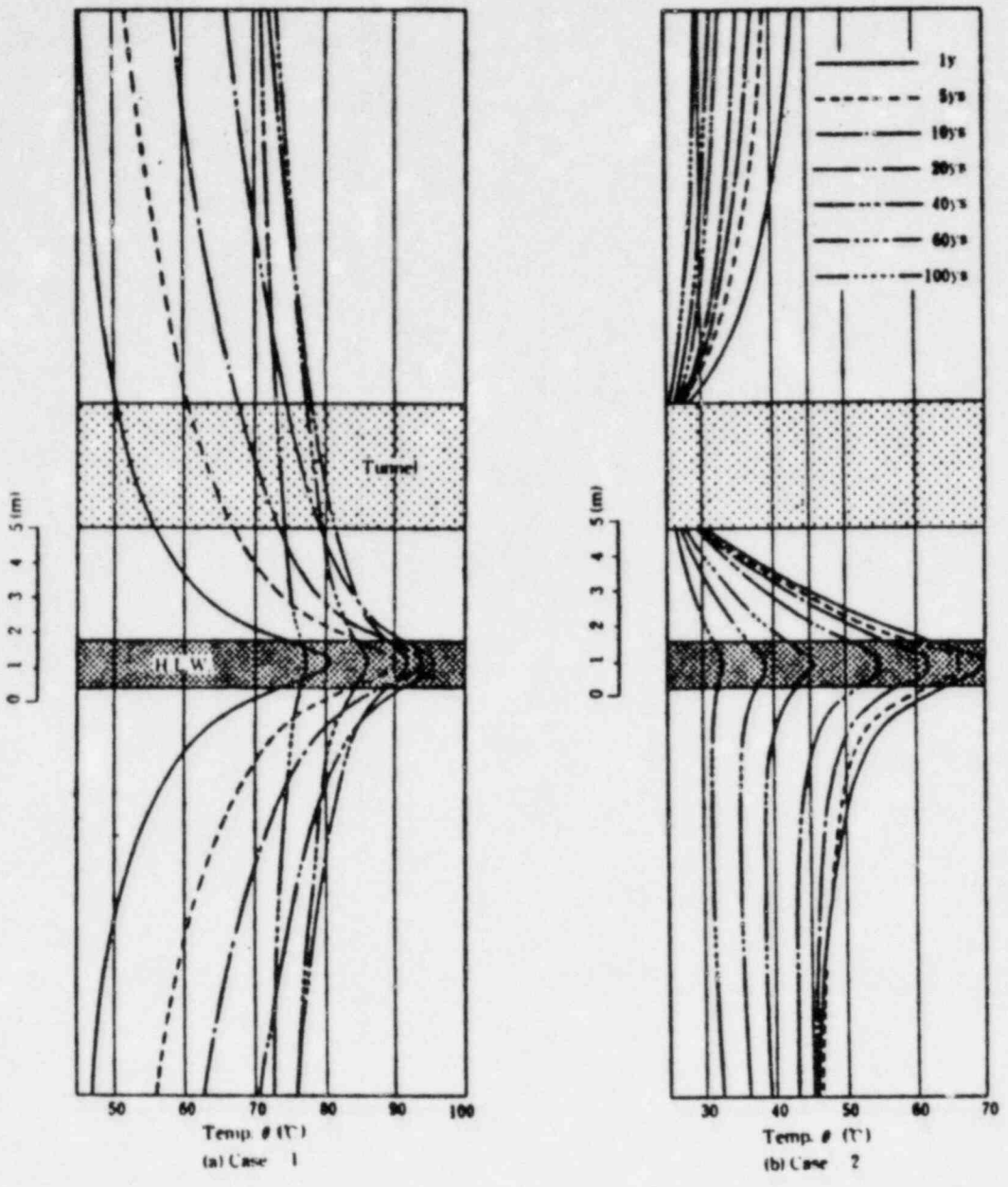

Fig. 4-13 Vertical profile of temperature along the centerline of the tunnel at various time after disposal

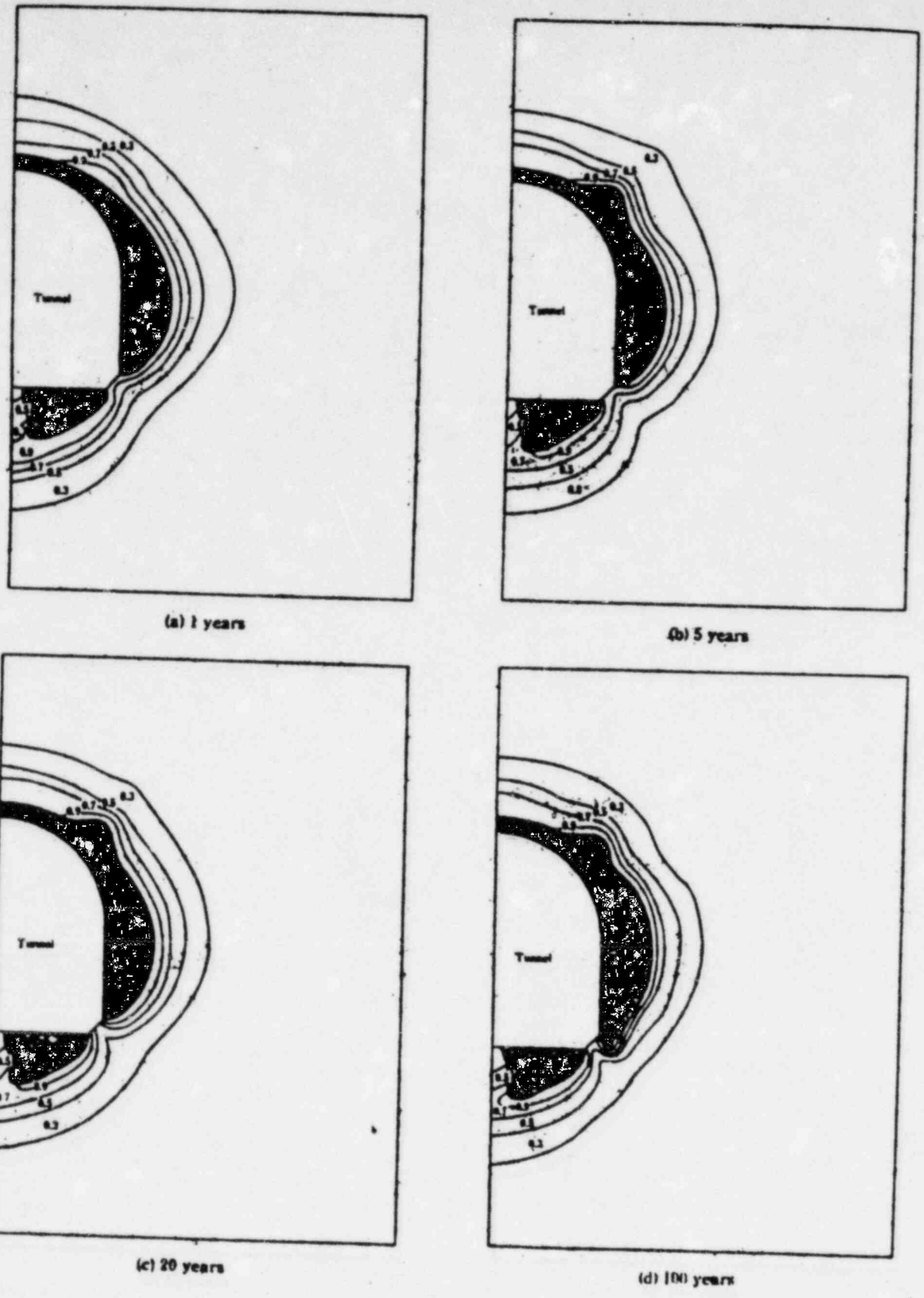

Fig. 4-14 The region of strength failure at various time after disposal (Case 2)

5. Preparation of Testing Apparatus in WASTEF

M. Senoo

Construction of the WASTEF, which provides hot cells to perform demonstrative safety tests of solidified HLW products with actual wastes, were completed in the latter term of 1981.[1] The main flow in WASTEF is planned as follows (Fig. 5-1). First, high-level liquid waste is transfered from a reprocessing facility and solidified by a vitrification apparatus. Using the vitrified products, safety tests for storage and disposal of HLW products will be carried out with following apparatus : a storage test apparatus, a canning and decontamination apparatus and gamma scanning detector in No. 1 cell, a vitrification apparatus in No. 2 cell, a disposal test apparatus and sample preparation apparatus in No. 3 cell, property measurement apparatus in No. 4 cell, an alpha radiation test apparatus in No. 5 cell and a microscope and a radiation detector in lead cell.

Allmost all testing apparatuses were prepared in the first term of 1982. After carrying out experiments with non-active simulated wastes, hot tests with active simulated wastes will be started in the latter term of 1982.

Reference

1) Tashiro, S., et al. ; Conceptual Design of the Waste Safety Testing Facility (WASTEF), JAERI-M 8485(1979)

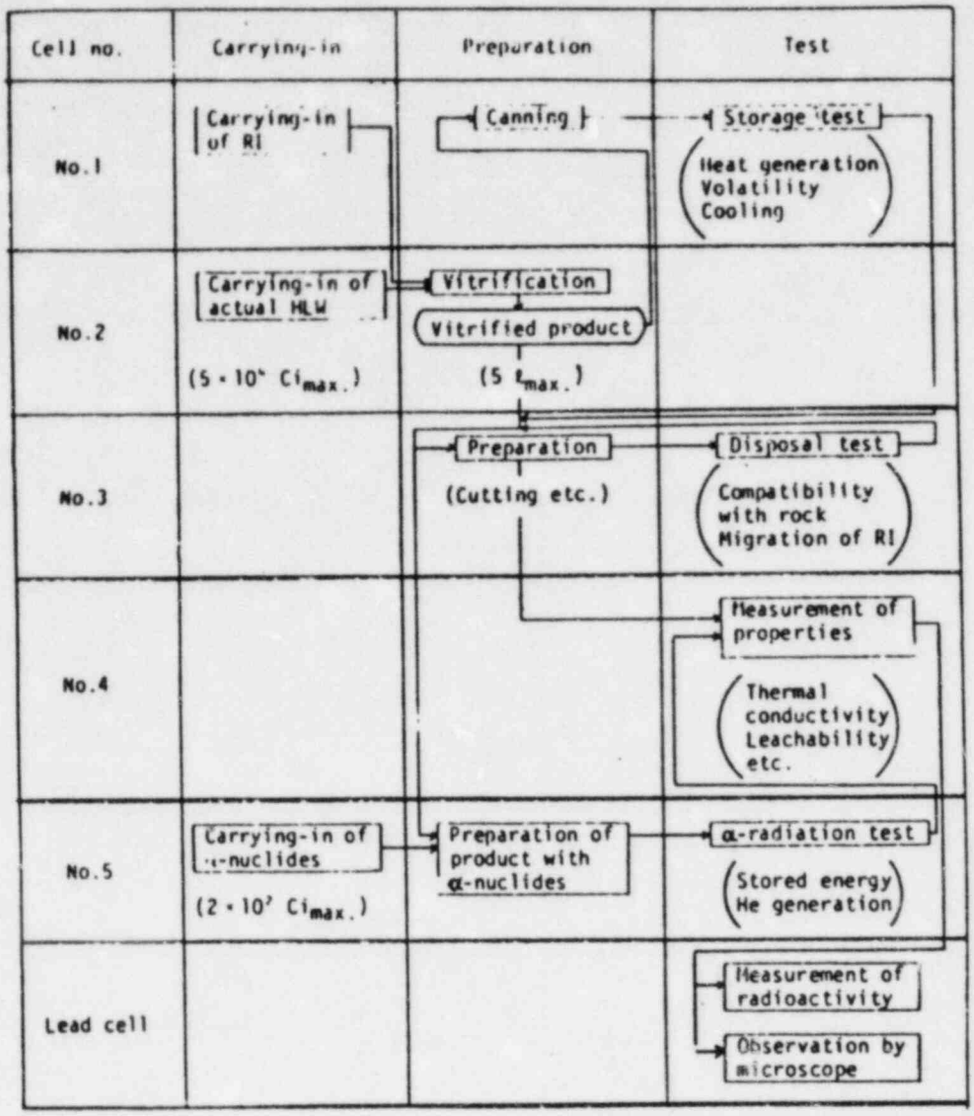

Fig. 5-1 Flow charts of tests in WASTEF

Acknowledgement

The editor and authors are grateful to Dr. K. Araki (Dupty Division Head, previous chief of the laboratory) and Mr. K. Imai (Division Head) for their continuing interest and encouragement.

The editor and authors thank Dr. H. Nakamura (present chief of the laboratory) for his support.

Thanks are also due all other members of the laboratory and the WASTEF Operation Section for their support to the work.